MicroRNA-449 sustains cilia-related networks in the absence of transcription factor TAp73

Merit Wildung[1#], Tilman U. Esser[1#], Katie B. Grausam[2,3], Cornelia Wiedwald[1], Li Li[2], Jessica Zylla[2], Ann-Kathrin Guenther[4], Magdalena Wienken[5], Evrim Ercetin[1], Felix Bremmer[6], Orr Shomroni[7], Stefan Andreas[1], Haotian Zhao[2,3,8*] and Muriel Lizé[1,*]

 # = equal contribution; * = corresponding authors

1) **Molecular & Experimental Pneumology Group, Clinic for Cardiology and Pneumology, University Medical Center Goettingen, Germany**
2) **Cancer Biology and Immunotherapeutics Group, Sanford Research, Sioux Falls, South Dakota, USA**
3) **Division of Basic Biomedical Sciences, University of South Dakota, Sanford School of Medicine, Vermillion, South Dakota**
4) **Department of Genes and Behavior, MPI for Biophysical Chemistry, Goettingen, Germany**
5) **Institute of Molecular Oncology, University Medical Center Goettingen, Germany**
6) **Institute of Pathology, University Medical Center Goettingen, Goettingen, Germany**
7) **Microarray and Deep-Sequencing Core Facility, University Medical Center Goettingen, Germany**
8) **Department of Biomedical Sciences, New York Institute of Technology College of Osteopathic Medicine, Old Westbury, New York, USA**

Abstract

Motile cilia serve vital functions in development, homeostasis and regeneration. We recently demonstrated that TAp73 is an essential transcriptional regulator of respiratory motile multiciliogenesis. Here we show that TAp73 is expressed in multiciliated cells (MCCs) of diverse tissues. Analysis of *TAp73*$^{-/-}$ animals revealed that TAp73 regulates *Foxj1*, *Rfx2/3*, axonemal dyneins *Dnali1* and *Dnai1*, plays a pivotal role in the generation of MCCs in reproductive ducts, and contributes to fertility. However, TAp73 is dispensable for brain MCCs, and robust activity from cilia-related networks is maintained in *TAp73*$^{-/-}$. Consistent with *TAp73*$^{-/-}$, its target *miR34bc* was reduced, whereas strong and specific induction of *miR449* was observed, along with an increase in *E2f4* that induced transcriptional response from *miR449* genomic regions. Depletion of both *TAp73* and *miR449* resulted in defective multiciliogenesis in the brain and hydrocephalus, indicating that miR449 and potentially additional pro-ciliogenic factors cooperate with TAp73 to ensure brain multiciliogenesis and CP development.

Introduction

Cilia are hair-like appendages protruding from the cell membrane into the surrounding environment. While single immotile primary cilia are a common organelle of most mammalian cells, motile cilia are restricted to a subset of cell types, including multiciliated cells (MCCs) lining brain ventricles, the tracheal, bronchial and oviduct epithelium as well as the epithelium of the efferent duct (ED) in the male reproductive tract (Spassky & Meunier, 2017).

Motile multiciliogenesis requires precise regulation of the production, transport and assembly of a large amount of different structural components, a process critically dependent on a hierarchical network of transcriptional and posttranscriptional regulators (Choksi, Lauter, Swoboda, & Roy, 2014). Geminin Coiled-Coil Domain Containing 1 (GEMC1) (Arbi et al., 2016; Terré et al., 2016; Zhou et al., 2015) and multiciliate differentiation and DNA synthesis associated cell cycle protein (MCIDAS or Multicilin) (Boon et al., 2014; Ma, Quigley, Omran, & Kintner, 2014; Stubbs, Vladar, Axelrod, & Kintner, 2012), members of Geminin family, are early regulators of MCC fate downstream of the NOTCH pathway. Inhibition of the NOTCH pathway e.g. by microRNA-449 (miR449) is required for multiciliogenesis through de-repression of the transcriptional network of *GEMC1*, *MCIDAS*, E2F transcription factors (*E2F4*, *E2F5*), forkhead box J1 (*FOXJ1*), and v-myb avian myeloblastosis viral oncogene homolog (*MYB)* (Danielian et al., 2007; Danielian, Hess, & Lees, 2016). Disturbance of the molecular circuit leads to defective multiciliogenesis and ciliopathies in the airways, reproductive tracts and the brain.

Transformation related protein 73 (*Trp73*) is a member of the p53 family with distinct isoforms generated from two alternative promoters: isoforms with N-terminal transactivation domain (TAp73), and N-terminally truncated dominant-negative isoforms (ΔNp73). Recently, we and others showed that TAp73 is essential for airway multiciliogenesis (Marshall et al., 2016; Nemajerova et al., 2016). Gene expression analyses and chromatin immunoprecipitation (ChIP) identified TAp73 as a critical regulator of multiciliogenesis: TAp73 acts downstream of E2F4/MCIDAS, and regulates the expression of *FOXJ1*, *RFX2,* and *RFX3* in pulmonary tissues (Blatt, Yan, Wuerffel, Hamilos, & Brody, 1999; Brody, Yan, Wuerffel, Song, & Shapiro, 2000; Chen, Knowles, Hebert, & Hackett, 1998; Nemajerova et al., 2016; Yu, Ng, Habacher, & Roy, 2008).

The fallopian tube (FT) of the female reproductive tract consists of the isthmus, the ampulla, and the infundibulum. MCCs here possess hundreds of motile cilia beating in a wave-like manner that, along with musculature contraction, moves the oocyte or zygote towards the uterus (**Figure 1B**) (Crow, Amso, Lewin, & Shaw, 1994; Lyons, Saridogan, & Djahanbakhch, 2006; Raidt et al., 2015). Defects in ciliary functions may lead to ectopic pregnancy or infertility (Lyons et al., 2006; Vanaken et al., 2017). In the male reproductive tract, MCCs in the efferent ducts (EDs) transport the spermatozoa from testis to epididymis (**Figure 1D**) (Ilio & Hess, 1994; Lambot et al., 2009).

Multiciliated cells (MCCs) in the brain can be found in a single layer of ependymal cells facing the ventricles and choroid plexus (CP) (**Figure 1F**). The CP epithelium, a specialized secretory epithelium that secretes cerebrospinal fluid, arise from monociliated progenitors in the roof plate

around embryonic day (E) 12 (M. P. Lun et al., 2015; Silva-Vargas, Maldonado-Soto, Mizrak, Codega, & Doetsch, 2016). Ependymal cells in mice are specified around day E16 and form multiple motile cilia on the apical surface after birth to facilitate cerebrospinal fluid movement (Melody P. Lun, Monuki, & Lehtinen, 2015; Spassky et al., 2005). Defects in the ependymal and CP lineages are implicated in aging, hydrocephalus, and brain tumors (Del Bigio, 2010; Li et al., 2016).

In this study, we detected robust TAp73 expression in MCCs in diverse tissues. Consistently, *TAp73* loss leads to a profound reduction of multiciliogenesis in the oviduct and EDs, and a significant loss of activity in TAp73-dependent transcriptional network. However, *TAp73* is dispensable for MCCs in the brain that maintain a robust multiciliogenesis program. Molecular studies revealed significant alterations in pro-ciliogenic *miR-34/449* family in *TAp73*$^{-/-}$ brain: reduced expression of TAp73 target *miR34bc* concurrent with strong *miR449* induction, suggesting that *miR449* induction might partially rescue brain ciliogenesis in the absence of *TAp73*. Indeed, loss of both *TAp73* and *miR449* leads to a dramatic loss of multiciliogenesis in the CP and severe hydrocephalus. Therefore, the molecular network governing multiciliated cell fate is subjected to tissue-specific feedback modulation.

Results

TAp73 is expressed in diverse multiciliated epithelia in development and adulthood

We and others previously showed that TAp73 expressed in respiratory epithelia controls multiciliogenesis (Marshall et al., 2016; Nemajerova et al., 2016). However, little is known about the expression and function of *TAp73* in other multiciliated cell types. To this end, quantitative PCR with reverse transcription (RT-qPCR) revealed abundant *TAp73* mRNA in ciliated tissues including efferent ducts (EDs), fallopian tubes (FTs), and brain ventricles/choroid plexus (CP), in addition to the testis as previously described (Holembowski et al., 2014; Inoue et al., 2014), (**Figure 1A**). In humans, we identified nuclear localization of TAp73 in EDs and FTs (**Figure 1B-E**). In mice, TAp73 expression was detected in ependymal and CP epithelial cells (**Figure 1 F and G**). During development, proliferative progenitors (KI-67^{+}) are present in hindbrain roof plate, whereas post-mitotic cells expressing Aquaporin 1 (AQP1) are detected in CP epithelium (KI-67^{-}/AQP1^{+}) (**Figure 1H**). Notably, a portion of the roof plate exists between the progenitors and CP epithelium that remains undifferentiated after cell cycle exit (KI-67^{-}/AQP1^{-}) (**Figure 1H**). In contrast to progenitors with solitary primary cilium, the “transition” zone is comprised of MCCs that exhibit p73 expression at day E14.5 (**Figure 1I**). Altogether, these data suggest a role for TAp73 in multiciliogenesis in reproductive tracts and the brain.

Wildung et al. Fig. 1

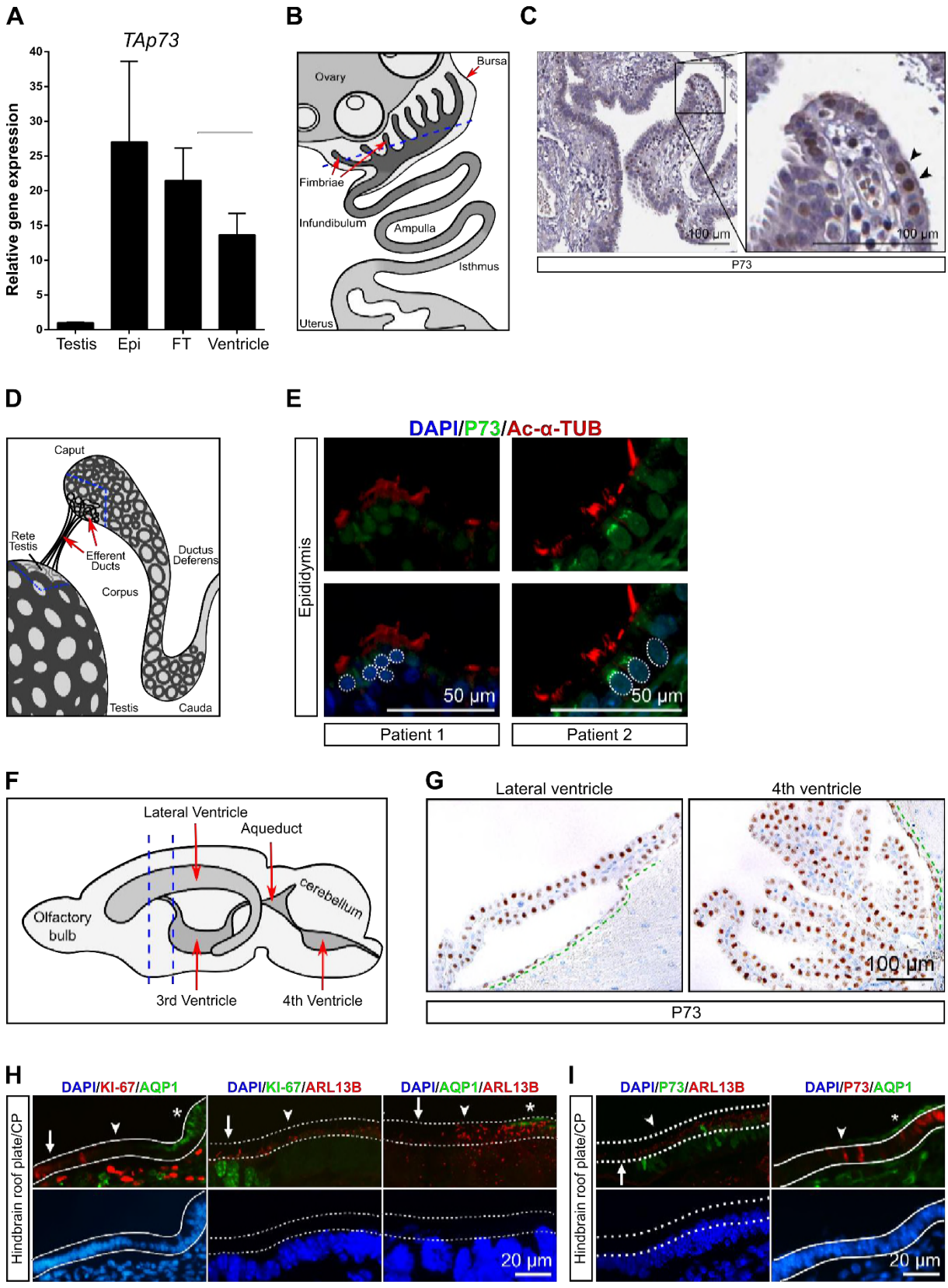

130

Legend to Figure 1. TAp73 is expressed in diverse multiciliated epithelial cells. (**A**) Quantitative reverse transcription PCR (RT-qPCR) analysis of *TAp73* expression in the testis, epididymis (Epi), fallopian tube (FT) and brain ventricle of wild type adult mice. Expression levels relative to *TAp73* expression in testis are shown (*n*=3, mean ± SEM). (**B**) Schematic illustration of fimbriae and fallopian tube that connect ovary and uterus**.** (**C**) The expression of P73 is shown in human fallopian tube. Boxed region (left) is shown in higher magnification (right) with $P73^{+}$ cells marked by arrowheads. Images were obtained from the Human Protein Atlas (https://www.proteinatlas.org/ENSG00000078900-TP73/tissue/fallopian+tube). (**D**) Schematic illustration of efferent ducts that connects testis and epididymis. (**E**) The expression of P73 (green) and axonemal markers acetylated alpha tubulin (Ac-α-TUB, red) is shown in human efferent ducts. White bracket circles delineate P73 nuclear staining in merged pictures. DAPI staining (blue) marks nuclei. (**F**) Schematic illustration of murine brain with different ventricles marked by arrows. Blue dotted lines illustrate coronal plane used for brain slices. (**G**) The expression of TAp73 is shown in lateral and 4^{th} ventricles of wild type adult mice. Notice that both ependymal and choroid plexus (CP) cells express TAp73. Green dotted lines demarcate ventricles lined with ependymal cells. (**H**) The expression of KI-67, Aquaporin (AQP1, green), and ARL13B (red) in wild type hindbrain roof plate/CP at embryonic (E) day E14.5. Notice that $KI\text{-}67^{+}$ roof plate progenitors, and $AQP1^{+}$ CP epithelial cells are spatially separated. ARL13B labels monociliated roof pate progenitors and multiciliated CP epithelial cells. White lines demarcate roof pate epithelium ($KI\text{-}67^{+}/AQP1^{-}$, arrows), CP epithelium ($KI\text{-}67^{-}/AQP1^{+}$, asterisks), and “transition zone” ($KI\text{-}67^{-}/AQP1^{-}$, arrowheads) in which MCCs appear. Dotted lines mark apical surface with cilia. DAPI staining (blue) labels nuclei. (**I**) Expression of TAp73, AQP1 (green), and ARL13B (red) in wild type hindbrain roof plate/CP at day E14.5. Dotted lines mark apical surface of roof plate ($TAp73^{-}$, arrow) and transition zone ($TAp73^{+}$, arrowhead). White lines mark transition zone ($TAp73^{+}/AQP1^{-}$, arrowhead) and CP epithelium ($TAp73^{+}/AQP1^{+}$, asterisk). DAPI staining (blue) labels nuclei.

***TAp73* is crucial for the molecular circuit of multiciliogenesis in efferent ducts**

Loss of *TAp73* leads to male infertility that has been attributed to defective spermaocyte production (Holembowski et al., 2014; Inoue et al., 2014). However, flagellated and motile spermatocytes are present in *TAp73*$^{-/-}$ mice, though at markedly reduced levels (**Figure 2A; Figure 2–video supplement 1A-D**), suggesting that additional defects as a result of *TAp73* loss may contribute to infertility in these mice. The multiciliated epithelium of the ED is involved in gamete transport from the testis to the epididymis, sperm concentration and maturation (Hess, 2002; Ilio & Hess, 1994), all essential aspects of male fertility (Dacheux & Dacheux, 2013). Indeed, though no gross morphological differences were observed in EDs between control and *TAp73* knockout (KO) animals (**Figure 2B**), staining of the cilia components acetylated alpha-tubulin (Ac-α-TUB) and axonemal dynein DNAI1 revealed a dramatic reduction in the number and length of cilia in the ED of mutant mice (**Figure 2C and D**), resembling the loss of airway cilia in these mice. ChIP followed by quantitative PCR (ChIP-qPCR) revealed significant enrichment of TAp73 in genomic loci of *FOXJ1*, axonemal dyneins *DNALI1* and *DNAI1* (**Figure 2E;** ChIPseq track depicted in **Figure 2–figure supplement 1**). Accordingly, the expression of *Dnali1* and *Dnai1, as well as FoxJ1* and *Rfx2*/3 was reduced or almost completely lost in *TAp73* KO animals (**Figure 2F-H**). Together, our results indicate that TAp73 directs *Dnali1* and *Dnai1* in addition to known critical nodes including *Foxj1*, *Rfx2* and Rfx*3* in EDs.

Wildung et al. Fig. 2

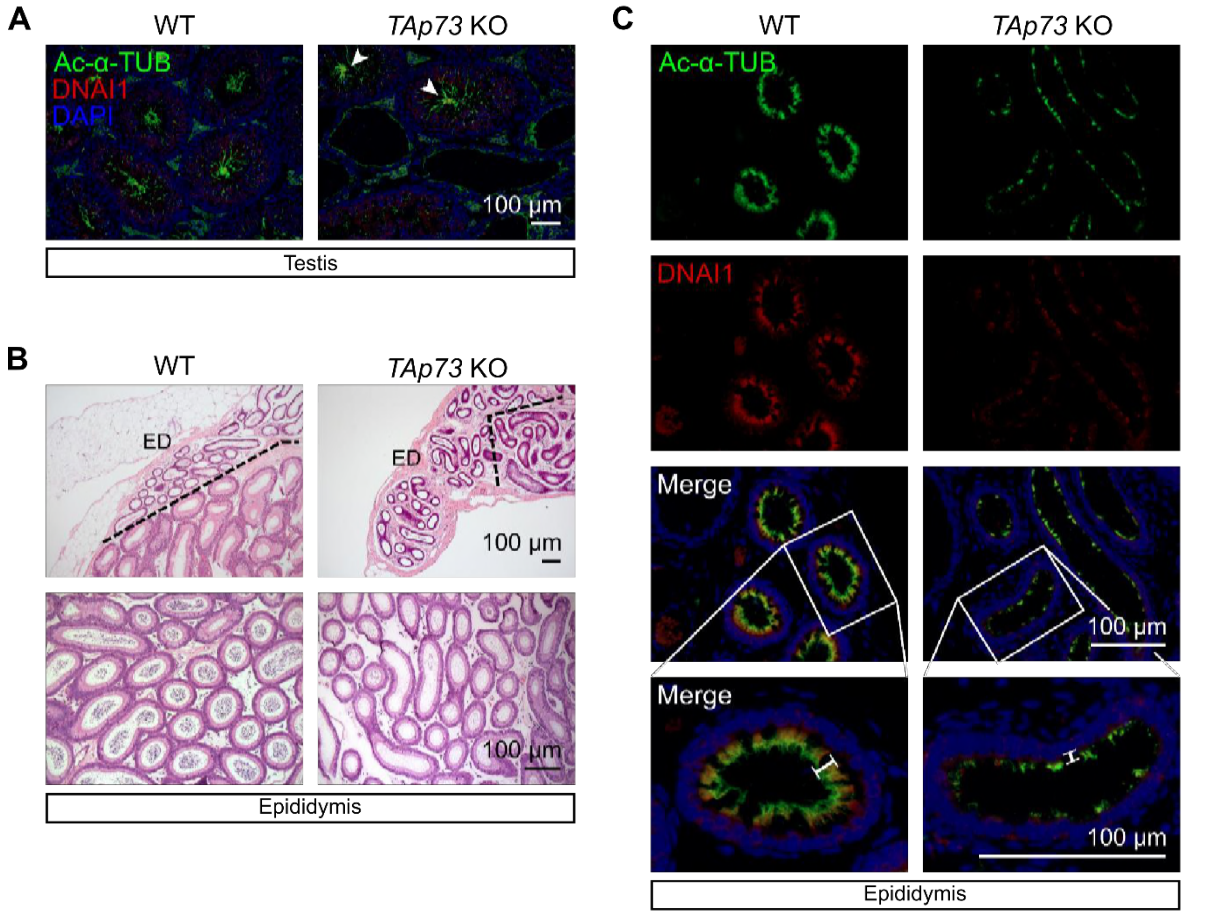

195

196 **Legend to Figure 2.** TAp73 controls motile multiciliogenesis in male reproductive tract. (**A**)
197 Representative images of the expression of Ac-α-TUB (green) and DNAI1 (red) are shown in
198 testis of wild type (WT) and *TAp73* knockout (KO) mice. DAPI staining (blue) labels nuclei. Notice
199 the presence of flagellated spermatocytes in *TAp73* KO testis. (**B**) Representative images of
200 hematoxylin and eosin (H&E) staining of epididymis sections in WT and *TAp73* KO animals.
201 Bracket lines demarcate the border of efferent duct (ED) and epididymis magnified in lower panel.
202 Notice that *TAp73* KO mice lack mature spermatocytes in distal epididymis. (**C**) Representative
203 images of the expression of Ac-α-TUB (green) and DNAI1 (red) are shown in efferent ducts of
204 WT and *TAp73* KO mice. DAPI staining (blue) labels nuclei. Boxed regions are magnified illustrate
205 cilia length (white bars). (**D**) Quantitation of Ac-α-TUB and DNAI1 signals normalized to epithelial
206 length shown in (**C**) (*n*=6 images from 3 WT mice; *n*=11 images from 4 *TAp73* KO mice). (**E**)
207 Chromatin immunoprecipitation was performed for Saos2 cells transfected with TAp73α, TAp73β,
208 and control empty vector. Binding of TAp73α (white bars) and TAp73β (black bars) to genomic
209 regions of *FOXJ1*, *DNALI1* and *DNAI1* is compared with that of control vector (grey bars) using
210 targeted quantitative PCR (*n*=3 for each antibody/gene pair shown, mean ± SEM, Genomic
211 regions examined are illustrated in Figure 2 - Figure supplement 1 (Koeppel et al., 2011).
212 Immunoblot analysis of the expression of axonemal dyneins DNALI1 and DNAI1, TAp73, and P73
213 isoform lacking N-terminal (**Δ**Np73) in testis (**F**) and epididymis (**G**) of WT and *TAp73* KO animals.
214 β-actin (**F**) and Heat shock cognate 71 kDa protein (HSC70, **G**) serve as a loading control. (**H**)
215 RT-qPCR analysis of *Dnali1, Foxj1* and *Rfx2 and Rfx3* expression in efferent ducts from WT
216 (empty bars) and *TAp73* KO (black bars) mice (*n*=3 samples/genotype, mean ± SEM).
217

Wildung et al. Fig. 2 - Figure supplement 1

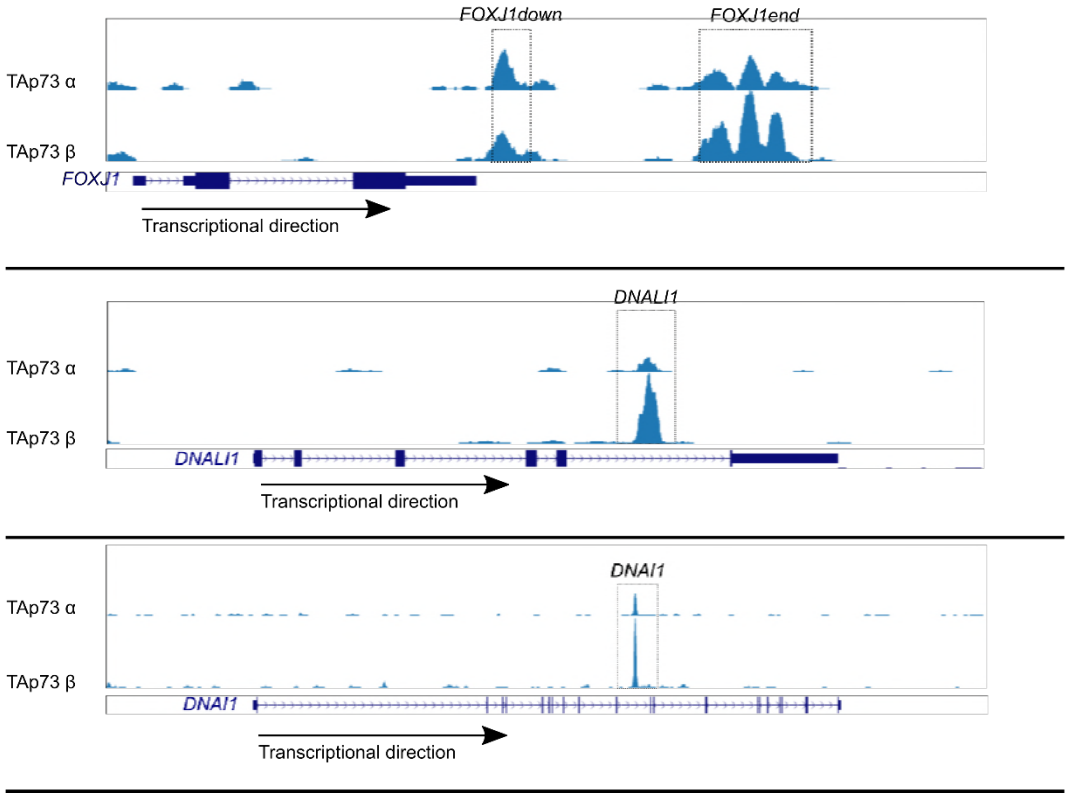

Legend to Figure 2–figure supplement 1. TAp73 is associated with ciliary genes expressed in male and female reproductive tracts. TAp73 binding at *FOXJ1*, *DNALI1* and *DNAI1* genomic loci is shown in results from ChIPseq (Koeppel et al., 2011), Geo accession no. **GSE15780**). Boxed regions mark genomic loci enriched with TAp73 binding and validated by quantitative PCR following ChIP (ChIP-qPCR) in **Figure 2E**.

TAp73-driven network of transcription factors regulates multiciliogenesis in fallopian tubes

Though female infertility associated with the loss of *TAp73* is thought to arise from the failure of oocytes release from the ovary and progression along FTs (Tomasini et al., 2008) (**Figure 1B**), it remained unclear how *TAp73* loss affects the gamete transport. To address this, we examined the FTs of *TAp73* KO animals and found a profound reduction in cilia coverage in oviduct epithelium despite normal tubal morphology (**Figure 3A and B**). Similar to observations in *TAp73*$^{-/-}$ EDs, protein products of genes bound by TAp73 (**Figure 2E**) FOXJ1, DNAI1 and DNALI1 (all expressed in the human FTs, cf. **Figure 3–figure supplement 1)** and transcript products of *Dnali1*, *Foxj1*, *Rfx2* and *Rfx3* were significantly reduced in *TAp73*$^{-/-}$ FTs (**Figure 3C and 3D respectively**), consistent with loss of TAp73-driven multiciliogenesis program. Further evaluation

of smooth muscle contraction pattern in FTs revealed no difference between control and TAp73 KO animals (**Figure 3–video supplement 1A and B**). Therefore, these data indicate that loss of TAp73 leads to reduced multiciliogenesis in the oviduct that may cause defective oocyte transport (Tomasini et al., 2008).

Wildung et al. Fig. 3

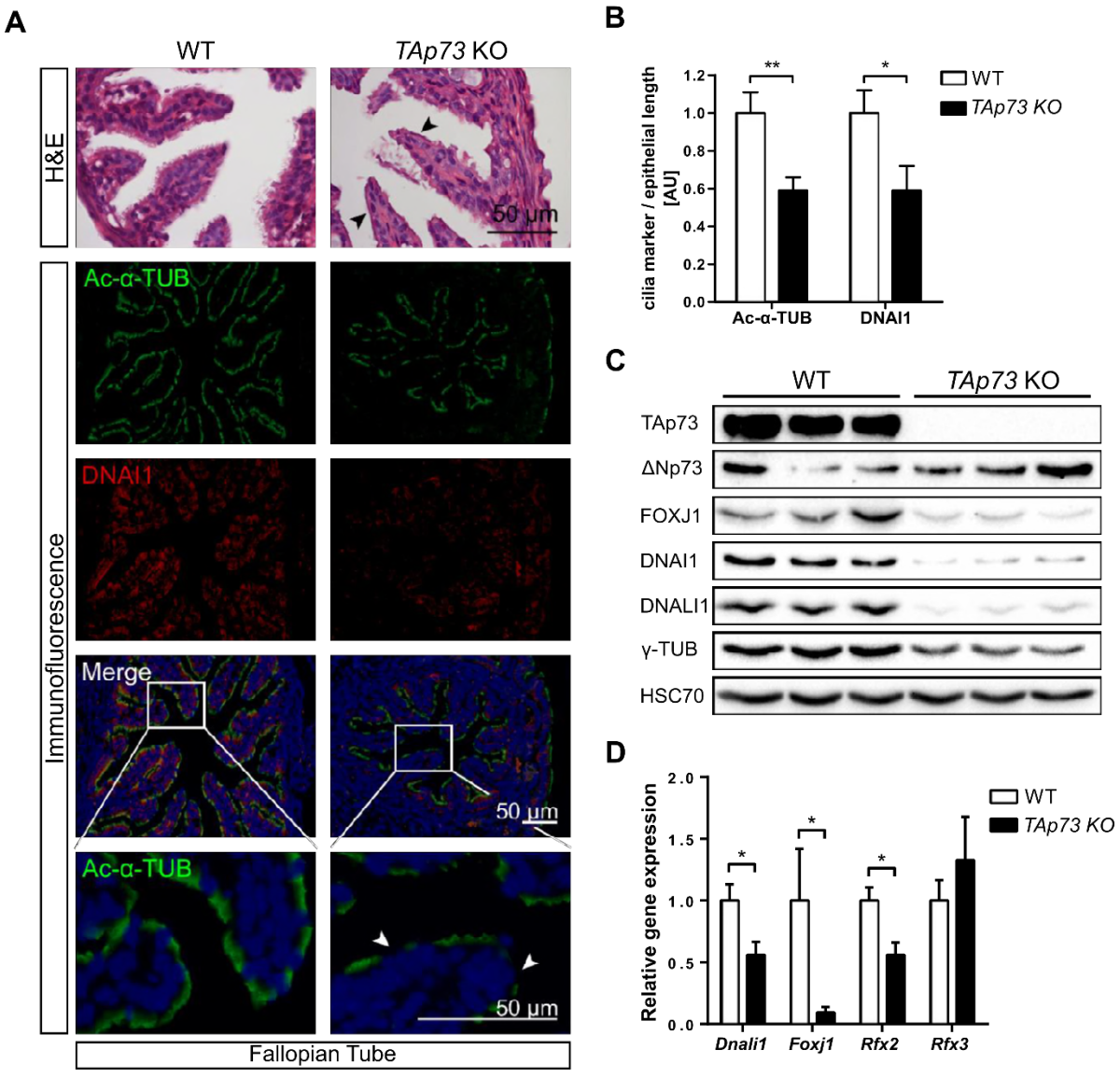

Legend to Figure 3. TAp73 controls motile multiciliogenesis in oviduct. (**A**) Representative images of H&E staining of fallopian tube are shown in WT and *TAp73* KO animals (upper panel). The expression of Ac-α-TUB (green) and DNAI1 (red) is shown in fallopian tube of WT and *TAp73* KO mice (lower panels). Boxed regions are magnified (lower panel). Arrowheads illustrate non-ciliated segments of fallopian tube of *TAp73* KO mice. DAPI staining (blue) labels nuclei. (**B**) Quantitation of Ac-α-TUB and DNAI1 signals shown in (**A**) and normalized to epithelial length

(*n*=9 images from 4 WT mice; *n*=7 images from 3 *TAp73* KO mice, mean ± SEM). (**C**) Immunoblot analysis of the expression of DNALI1, DNAI1, gamma tubulin (γ-TUB), FOXJ1, TAp73, and **Δ**Np73 in oviducts from WT and *TAp73* KO animals. HSC70 serve as a loading control. (**D**) RT-qPCR analysis of *Dnali1, Foxj1 Rfx2* and *Rfx3* expression in oviducts from WT (empty bars) and *TAp73* KO (black bars) mice (*n*=3 samples/genotype, mean ± SEM).

Note: Rfx3 primers do not span an intron and could thus theoretically amplify genomic sequence.

Wildung et al. Fig. 3 - Figure supplement 1

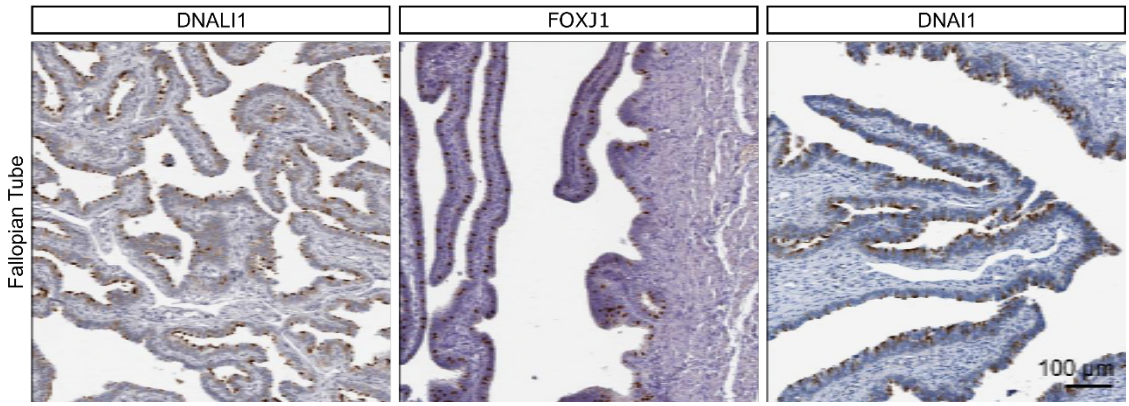

Legend to Figure 3–figure supplement 1. Human FT epithelia express DNALI1, FOXJ1 and DNAI1. Images retrieved from the Human Protein Atlas (DNALI1: http://www.proteinatlas.org/ENSG00000163879-DNALI1/tissue/fallopian+tube, FOXJ1: http://www.proteinatlas.org/ENSG00000129654-FOXJ1/tissue/fallopian+tube, DNAI1: http://www.proteinatlas.org/ENSG00000122735-DNAI1/tissue/fallopian+tube).

Multiciliogenesis in the brain is unaltered in the absence of *TAp73*

The expression of TAp73 in ependymal and CP epithelial cells (**Figure 1F-H**), along with recent studies suggesting the role of MCIDAS/E2F4 in multiciliogenesis of these cells (Kyrousi, Lalioti, Skavatsou, Lygerou, & Taraviras, 2016; Ma et al., 2014; Mori et al., 2017), led us to examine the role of *TAp73* in MCCs in the brain. Morphological and gene expression studies revealed no apparent defect in ependymal cells and the CP in *TAp73* KO brains and confirmed lack of P73 expression (**Figure 4A and B**). We performed staining for Ac-α-TUB and DNAI1, and cilia marker ADP-ribosylation factor-like 13b (ARL13B; (Caspary, Larkins, & Anderson, 2007) in lateral and 4th ventricles. In contrast to FT and EDs, our results showed that the number and length of cilia from ependymal and CP cells in *TAp73*$^{-/-}$ animals are similar to those of control animals (**Figure 4C, E; Figure 4–figure supplement 1A and B**). Consistently, ciliary beating and bead flow in cerebrospinal fluid appeared unaffected by *TAp73* KO (**Figure 4D; Figure 4–video supplement 1A and B**). Furthermore, no significant difference was observed in the expression of markers for epithelial differentiation of CP between control and *TAp73*$^{-/-}$ animals (**Figure 4–figure supplement 1C-F**). RT-qPCR analysis demonstrated comparable expression of *Dnali1* and *Foxj1* whereas increased *Rfx2* and *Rfx3* mRNA levels were observed in brain ventricles of *TAp73* KO mice (**Figure 4F**). Taken together, these results indicate that multiciliogenesis in the brain remains intact despite the loss of *TAp73*.

Wildung et al. Fig. 4

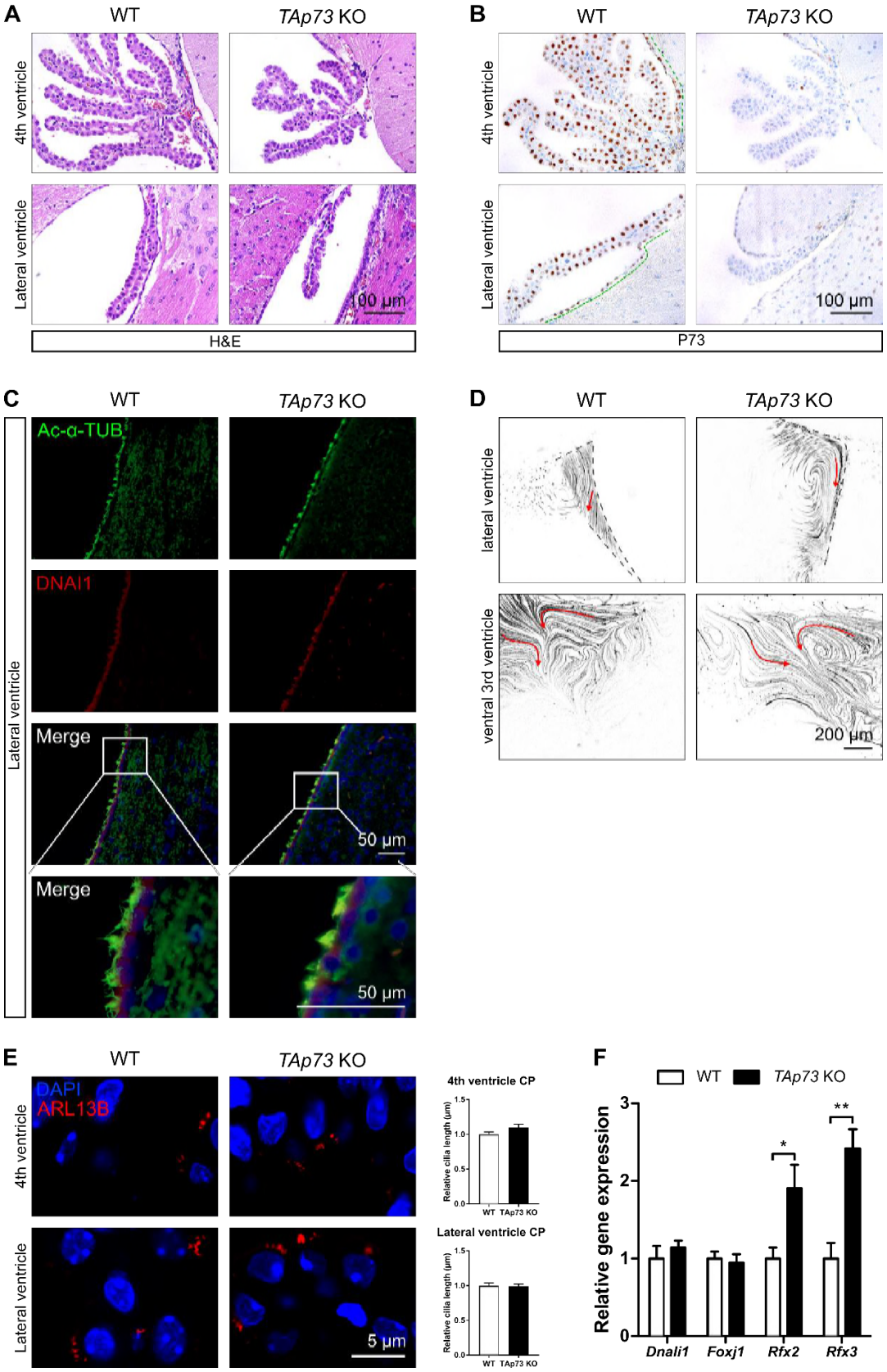

298

Legend to Figure 4. *TAp73* is dispensable for brain multi-ciliogenesis. (**A**) Representative H&E staining images are shown of ependymal and CP epithelial cells in hindbrain and lateral ventricle from WT and *TAp73* KO animals. (**B**) The expression of TAp73 is shown in ependymal and CP epithelial cells shown in (**A**). Notice that TAp73 expression is lost in these cells in *TAp73* KO mice. Green dotted lines mark demarcate ventricles lined with ependymal cells.(**C**) Representative images of the expression of Ac-α-TUB (green) and DNAI1 (red) in ependymal cells in lateral ventricle from WT and *TAp73* KO animals shown in (**A**). DAPI staining (blue) labels nuclei. Boxed regions are magnified to illustrate cilia on cell surface. (**D**) Quantitation of the movement of fluorescent beads along the ventricular system. Images of maximum intensity projections of representative movies of the lateral and the ventral 3rd ventricles are shown (*n*=3 for *TAp73*$^{-/-}$ mice; *n*=1 for TAp73$^{+/-}$ mice; and *n*=2 for WT mice). Red arrows mark the direction of bead flow. Bracket lines depict ependymal layer lining the ventricles. Refer to **Figure 4– Video supplement 1A-B** for examples of recording of ciliary beating. (**E**) The expression of cilia marker ARL13B (red) is shown in CP epithelial cells shown in (**A**). DAPI staining (blue) labels nuclei. Graphs show quantitation of average cilia length in CP epithelial cells shown in upper and lower panels. (**F**) RT-qPCR analysis of *Dnali1, Foxj1* and *Rfx2/3* expression in brain ventricles from wild type (empty bars) and *TAp73* KO (black bars) mice (*n*=3 samples/genotype, mean ± SEM).

Note: Rfx3 primers do not span an intron and could thus theoretically amplify genomic sequence.

Wildung et al. Fig. 4 - Figure supplement 1

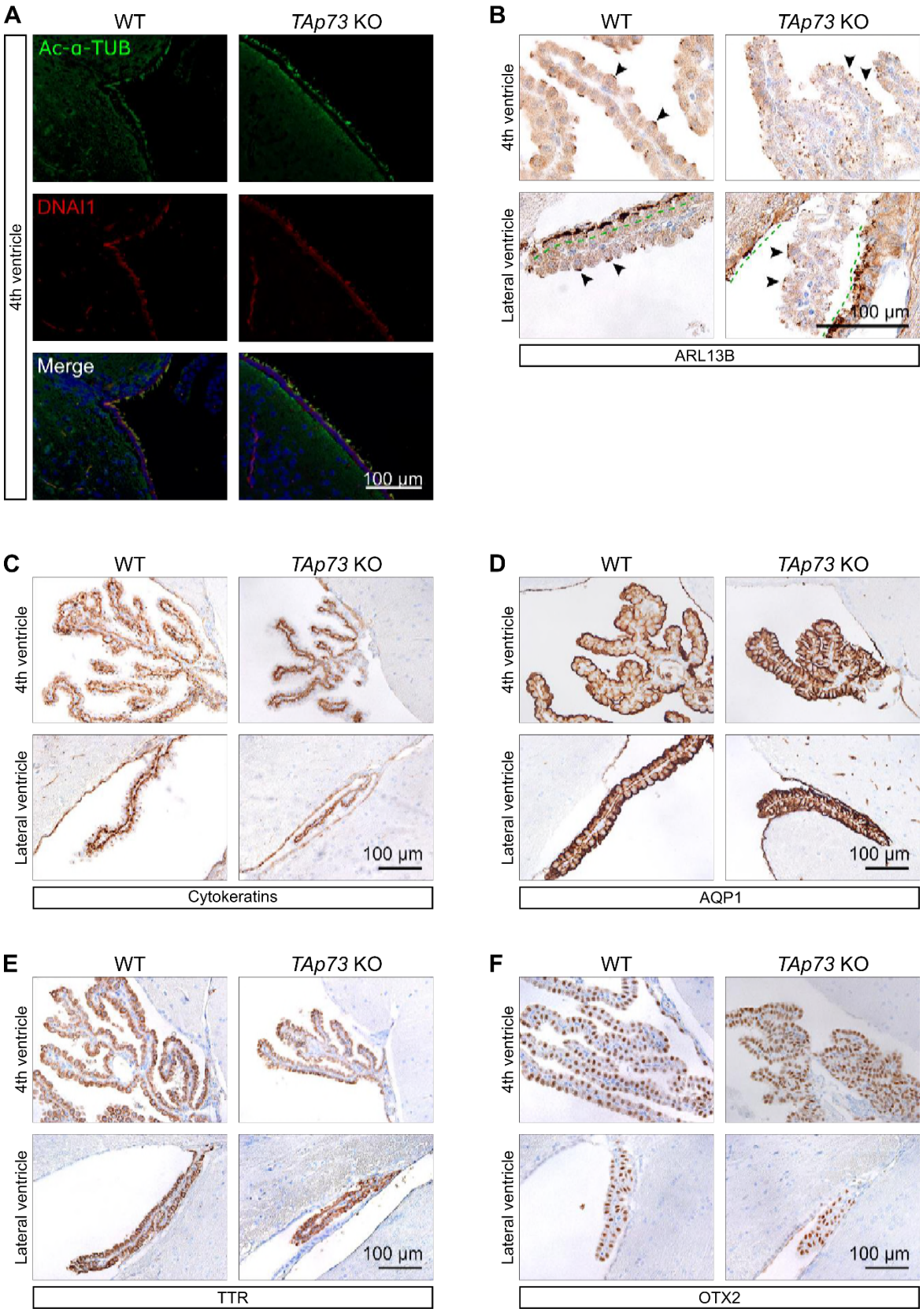

319

Legend to Figure 4–figure supplement 1. *TAp73* is dispensable for multiciliogenesis in the brain. (**A**) The expression of Ac-α-TUB (green) and DNAI1 (red) is shown in ependymal cells of the 4th ventricle from WT and *TAp73* KO animals. Representative images of the expression of ARL13B (**B**), cytokeratins (**C**), AQP1 (**D**), transthyretin (TTR, **E**), and Orthodenticle homeobox 2 (OTX2, **F**) are shown in CP epithelium of the 4th and lateral ventricles from WT and *TAp73* KO animals. Red dotted lines mark the boundary of lateral ventricles lined with ependymal cells.

TAp73 functions through posttranscriptional codes in brain multiciliogenesis

Besides transcription factors, TAp73 utilizes posttranscriptional mechanisms involving micro RNAs. Consistently, sequencing of small RNA species from brain ventricles revealed significant reduction in *miR34bc* (**Figure 5A;** complete small RNA sequencing results in **Figure 5–table supplement 1** and in GEO under accession number **GSE108385**), reminiscent of findings in *TAp73*$^{-/-}$ airways. Remarkably, our analysis also revealed a strong induction of microRNA cluster *miR449* (**Figure 5A; Figure 5–table supplement 1; GSE108385**), that together with *miR34bc* regulates multiciliogenesis in different tissues across species (Lizé, Herr, Klimke, Bals, & Dobbelstein, 2010; Marcet, Chevalier, Luxardi, et al., 2011; Marcet, Chevalier, Coraux, Kodjabachian, & Barbry, 2011; Song et al., 2014). In agreement, *miR449* is predominantly expressed in the CP, and increases significantly by over 10-fold upon *TAp73* loss in ventricles (**Figure 5B and C**) but not in FT nor ED preparations (**Figure 5–figure supplement 1**) (Redshaw, Wheeler, Hajihosseini, & Dalmay, 2009).

miR449 is known to suppress the NOTCH pathway, thereby activating the transcriptional cascade involving MCIDAS/E2Fs (Boon et al., 2014; Kyrousi et al., 2016; Marcet, Chevalier, Luxardi, et al., 2011; Stubbs et al., 2012; Terré et al., 2016). Though only a slight and non-significant increase in the expression of *Mcidas* was observed in brain ventricles after *TAp73* loss, the expression of *E2f4* in brain ventricles was significantly increased in *TAp73* KO mice compared to control animals (**Figure 5C**). Previous reports showed that *miR449* can be activated by E2F1 (Lizé, Pilarski, & Dobbelstein, 2010; X. Yang et al., 2009). Given the conserved binding motif of the E2F transcription factors, we isolated *miR449* genomic region (*miR449* is embedded in *CDC20B* gene) with putative E2F binding sites to assess interaction with MCIDAS/E2F4 in luciferase reporter assay. Indeed, *MCIDAS* alone or in combination with *E2F4* elicited strong transcriptional response from *miR449* locus, a reaction almost completely abolished by mutating the strongest of the three putative E2F binding sites (**Figure 5D and materials and methods Table 5**). This suggests that increased MCIDAS/E2F4 activity stimulates *miR449* expression in *TAp73* KO brain ventricles.

Wildung et al. Fig. 5

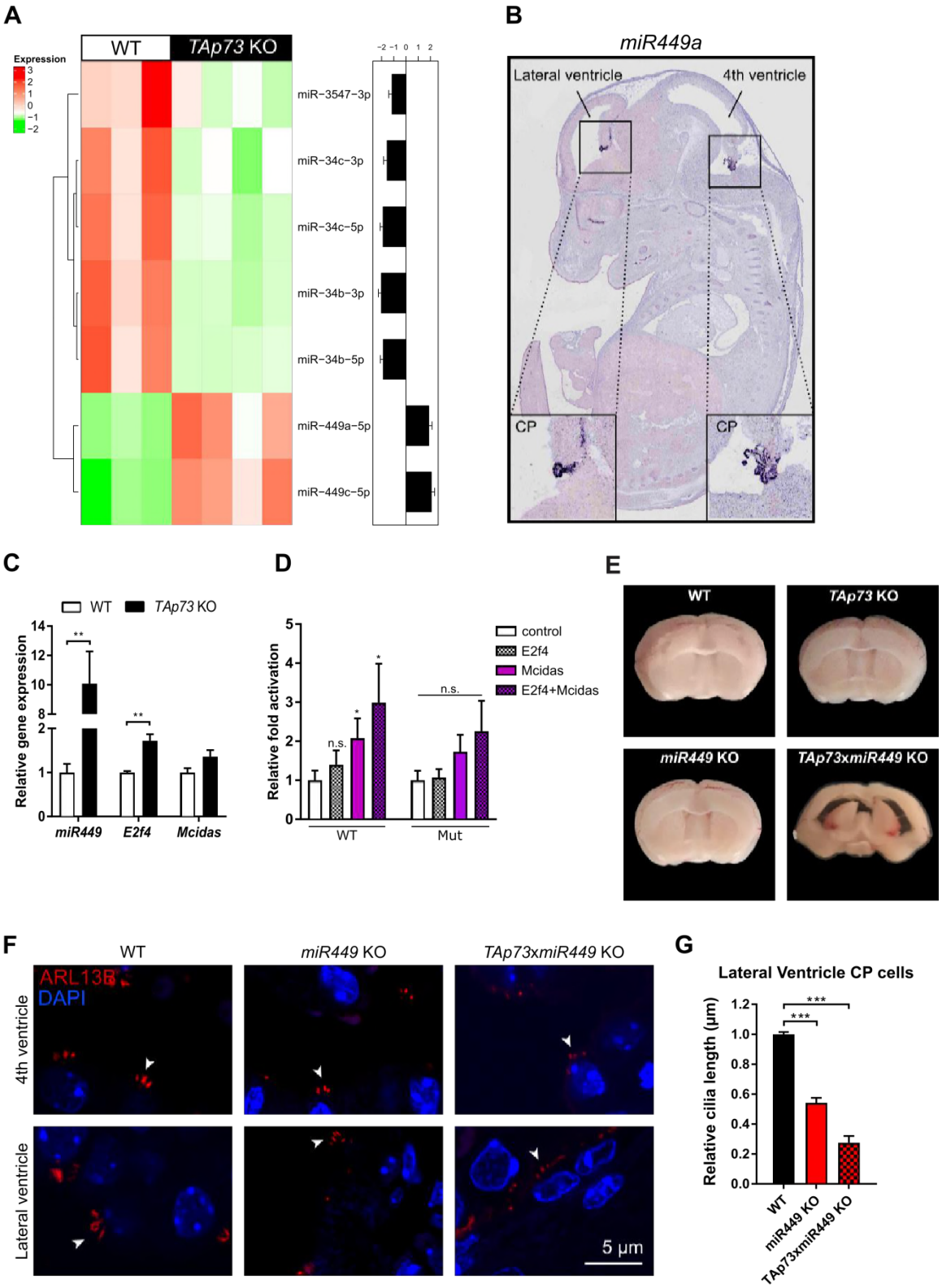

357
358

Legend to Figure 5. TAp73 functions through *mir-34/449* family in brain multiciliogenesis. (**A**) Hierarchical clustering of differentially expressed micro RNAs in brain ventricles between WT and *TAp73* KO mice (left panel, *n*=3 for WT mice, n=4 for *TAp73* KO mice, mean ± SEM, one-way ANOVA, FDR < 0.05, fold change is shown). Expression differences are plotted as $\log_2$ values for micro RNAs shown in heat map (right panel). Complete sRNA-seq data sets can be found in Gene Expression Omnibus (GEO) under accession number **GSE108385**. (**B**) *In situ* hybridization analysis of the expression of *miR449* in roof plate/CP at day E14.5 (http://www.eurexpress.org/ee/, (Diez-Roux et al., 2011). (**C**) RT-qPCR analysis of *miR449*, *E2f4*, and *Mcidas* in brain ventricles from WT (empty bars) and *TAp73* KO (black bars) mice (*n*=3 samples/genotype, mean ± SEM). (**D**) Luciferase assay of regulatory regions of *miR449* containing E2F binding motifs. *miR449* genomic sequences with three consensus E2F binding sites were identified (http://jaspar.binf.ku.dk/) and placed in front of a luciferase cassette. Deletion mutant (Mut) was created that lack the strongest consensus site but retains two milder E2F consensus sequences (**Materials and methods Table 5**). Wild type and mutant luciferase vectors were then co-transfected with empty vector (control, empty bars), or vectors expressing *E2F4* (checkered), *MCIDAS* (purple bars) or both (purple checkered bars). The results are shown as fold changes in luciferase activities relative to control vector (*n*=4, mean ± SEM). (**E**) Coronal brain slices as depicted by blue lines in **Figure 1F** are shown from WT, *TAp73* KO, *miR449* KO and *TAp73/miR449* double knockout (*TAp73xmiR449* KO) mice. Note that *TAp73xmiR449* KO mice display severe hydrocephalus. (**F**) Representative images of the expression of cilia marker ARL13B (red) are shown in CP epithelial cells of hindbrain and lateral ventricles in WT, *miR449* KO, and *TAp73xmiR449* KO mice. DAPI staining (blue) labels nuclei. (**G**) Quantitation of average cilia length of CP epithelial cells shown in (**F**) (*n*=9 images from 4 WT mice; *n*=7 images from 3 *TAp73* KO mice, mean ± SEM).

Wildung et al. Fig. 5 - Figure supplement 1

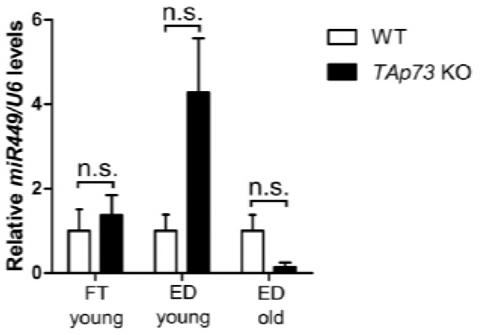

Legend to Figure 5–figure supplement 1. FTs and EDs of *TAp73* KO do not display significant increase in *miR449* expression.

Note: We cannot directly compare gene expression in "young" versus "old" ED cohorts due to age and preparation differences. However, this discrepancy fortifies the idea that, in contrast to the brain, there is no significant change in miR449 expression in response to TAp73$^{-/-}$ neither in FTs nor in EDs. Cohorts: FT young: n=4 WT and n=4 TAp73 KO; ED young: n=3 WT and n=5 TAp73 KO; ED old: n=4 WT and n=3 TAp73 KO.

Our data suggests that a crosstalk between MCIDAS/E2F4 and *miR449* may partially compensate for *TAp73* loss in brain multiciliogenesis. To address this, we performed deletion of *miR449* cluster in *TAp73* mutant background. Strikingly, *TAp73*$^{-/-}$*;miR449*$^{-/-}$ (aka *TAp73xmiR449* KO) mice developed severe hydrocephalus (**Figure 5E, Figure 5–figure supplement 2A**). Analysis of ARL13B expression revealed that, though *miR449* loss alone resulted in a significant decrease in the length of cilia in CP epithelial, a more pronounced reduction in cilia was observed in*TAp73xmiR449* KO mice (**Figure 5F and G; Figure 5–figure supplement 2B**). No significant difference was observed in the expression of genes normally found in CP epithelial cells among wild type, *TAp73* KO, *miR449* KO, and *TAp73xmiR449* KO animals (**Figure 5–figure supplement 2C-E**). Despite the role of NOTCH signaling in CP development and tumorigenesis (Bill et al., 2008; Li et al., 2016), RNAscope studies revealed similar expression of NOTCH pathway targets *Hes1* and *Hes5* in the roof plate of control, *miR449*$^{-/-}$ and *TAp73xmiR449* KO embryos at day E14.5 (**Figure 5–figure supplement 3**), indicating normal NOTCH pathway activity in the absence of *miR449*. Together, our data indicate that TAp73 utilizes the unique topology of its transcriptional network to communicate with *miR-34/449* family and other crucial regulators of motile multiciliogenesis e.g. *E2F4/MCIDAS* to regulate brain ciliogenesis (**Figure 6**).

Wildung et al. Fig. 5 - Figure supplement 2

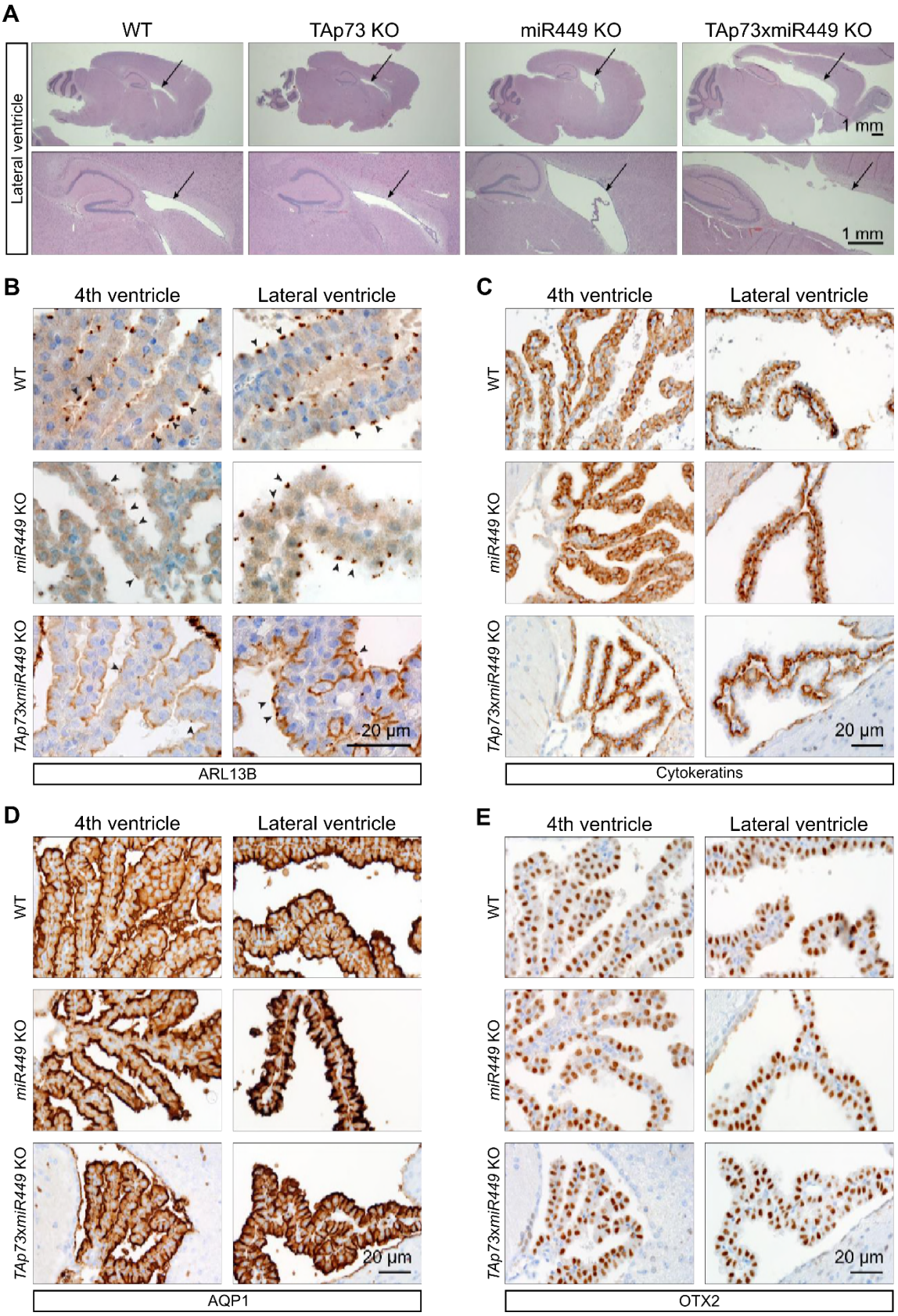

416

Legend to Figure 5–figure supplement 2. miR449 compensates loss of *TAp73* in brain multiciliogenesis. (**A**) Representative H&E stainings of WT, *TAp73* KO, *miR449* KO and *TAp73xmiR449* KO. Arrows point at ventricles, with TAp73xmiR449 KO displaying strong hydrocephalus. Representative images of the expression of ARL13B (**B**) cytokeratins (**C**), AQP1 (**D**), OTX2 (**E**) in the CP epithelium of the 4th and lateral ventricles from WT, *miR449* KO, and *TAp73xmiR449* KO mice.

Wildung et al. Fig. 5 - Figure supplement 3

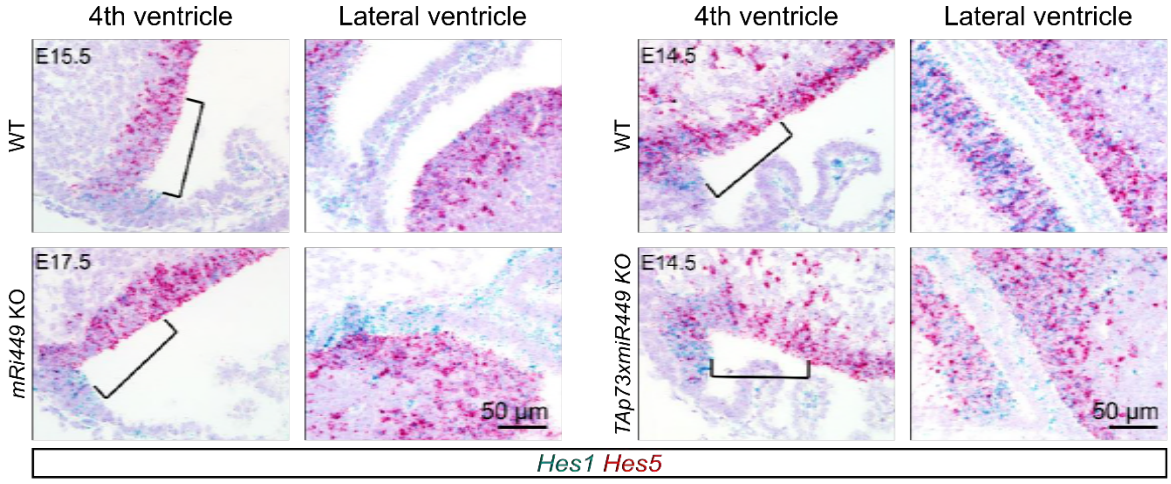

Legend to Figure 5–figure supplement 3. NOTCH signaling is unaltered in *miR449* KO and *TAp73xmiR449* KO developing ventricles. RNAscope analysis of the expression of NOTCH targets *Hes1* (blue) and *Hes5* (red) in 4th and lateral ventricles of WT, *miR449* KO, and *TAp73xmiR449* KO mice.

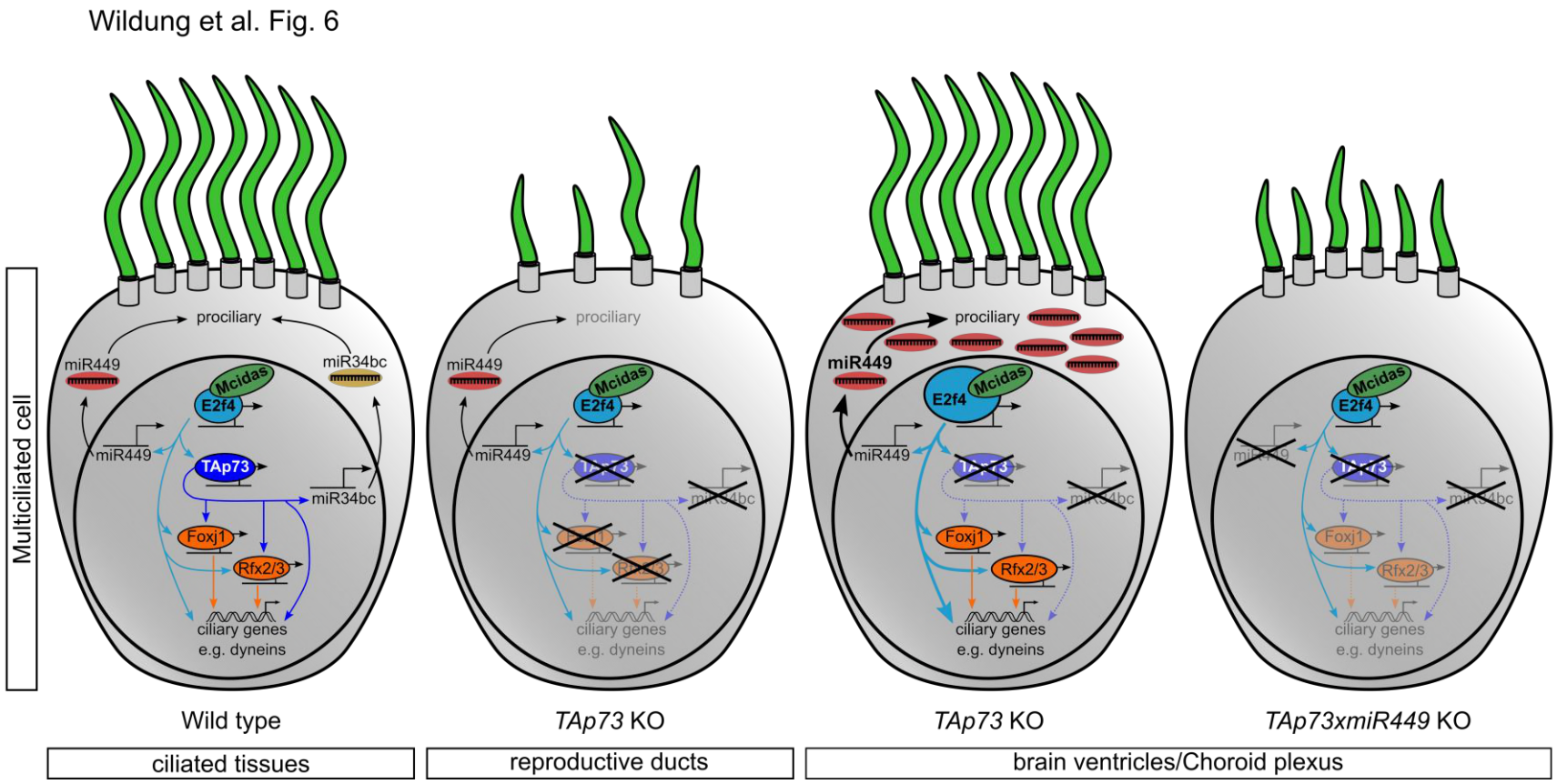

Legend to Figure 6. Schematic diagram of the molecular mechanisms of TAp73-driven multiciliogenesis in diverse tissues.

- TAp73-dependent transcriptional network, including dyneins, *miR34bc*, *Foxj1* and *Rfx2/3* factors, critically regulates multiciliogenesis in various ciliated tissues downstream of *E2f4*/*Mcidas*.
- In reproductive ducts TAp73 ensures the generation of MCCs and proper gamete and zygote transport, whereas loss of *TAp73* impairs fertility in male and female.
- *TAp73* is not essential for multiciliogenesis in the brain; however, *TAp73* loss leads to upregulation of pro-ciliogenic *E2f4* and its target *miR449*.
- Further removal of *miR449* in addition to *TAp73* loss leads to reduced cilia and severe hydrocephalus, indicating that miR449 partially compensates loss of *TAp73* in brain ciliogenesis.

Discussion

TAp73 activates a plethora of ciliogenic effectors to drive multiciliogenesis in the airways (Marshall et al., 2016; Nemajerova et al., 2016). The current study examines the role of TAp73-driven molecular circuit in MCCs of reproductive tracts and the brain. Our results revealed profound changes in both male and female reproductive tracts lacking *TAp73*, suggesting that infertility associated with TAp73 loss can be in part explained by cilia loss. The striking reduction in MCCs in *TAp73*$^{-/-}$ oviduct and EDs, together with diminished *Foxj1*, *Rfx2 and Rfx3* expression, is reminiscent of findings in respiratory epithelia of *TAp73* KO mice. The expression of dyneins *Dnai1* and *Dnali1*, both of which exhibit TAp73 binding in their genomic loci, is significantly reduced in mutant animals, indicating that they are part of TAp73-directed multiciliogenesis program in reproductive tracts.

The integrity of MCCs is critical for reproductive health. Disruption of transcriptional regulators of multiciliogenesis consistently leads to infertility in mice and in humans (Amirav et al., 2016; Terré et al., 2016), whereas fertility issues have been reported in female primary ciliary dyskinesia patients (Raidt et al., 2015; Vanaken et al., 2017). Importantly, *TAp73* is downregulated as women age (Guglielmino et al., 2011), whereas certain single nucleotide polymorphisms in *TP73* is associated with female patients over 35 years of age seeking *in vitro* fertilization treatment (Feng et al., 2011; Hu, Zheng, & Wang, 2011). Further studies using tissue-specific deletion of *TAp73* are necessary to delineate its role in reproductive motile cilia maintenance and fertility.

In *TAp73*$^{-/-}$ males, consistent with previous reports, we found partial degradation of the germinal epithelium and reduced sperm cell production (Holembowski et al., 2014; Inoue et al., 2014). However, although reduced in number, spermatocytes in *TAp73* KO are morphologically normal with beating flagella, raising questions about the underlying causes of sterility in these mice. The efferent ducts connecting testis and epididymis comprise multiciliated cells that are required for the transport of spermatozoa to their storage and maturation location. Our present work reveals that male sterility in mice with defective multiciliogenesis e.g. *TAp73*$^{-/-}$ mice can at least partially be attributed to defective ED epithelia.

During embryogenesis, robust *TAp73* expression is initiated at the onset of multiciliate differentiation of ependymal and CP epithelial cells. However, our data indicate that generation of multiciliated cells in the brain appears independent of *TAp73*, although we cannot exclude that *TAp73* KO generates more subtle defects in polarity or cilia orientation. In contrast to the dynamic TAp73-dependent program in the airways and reproductive tracts, the expression of *Foxj1, Rfx2 and Rfx3* in the *TAp73*$^{-/-}$ brain remains unaltered and exhibits a slight increase respectively, suggesting that other effectors maintain the molecular circuit to support MCCs.

Previous studies revealed robust expression of *GemC1* and *E2f/Mcidas*, all of which are capable of transcriptional activation of *Foxj1*, *TAp73* itself, and many other ciliogenic effectors e.g. *Rfx2* and *Rfx3*, in MCCs in the brain (Arbi et al., 2016; Boon et al., 2014; Kyrousi et al., 2016; Pefani et al., 2011; Stubbs et al., 2012). Indeed, E2F4/MCIDAS activity is induced in response to *TAp73*

loss, and therefore may facilitate brain multiciliogenesis in the absence of *TAp73*. In agreement, loss of either *E2F4* or *GemC1* leads to defect in MCC differentiation and hydrocephalus (Lindeman et al., 1998; Terré et al., 2016).

Though it is less clear how TAp73 loss results in enhanced MCIDAS/E2F activity, a quick look downstream of TAp73 provides some clues: a decrease of TAp73 target *mir34bc* accompanied by an increase in *miR449* in the absence of TAp73. *miR449* induction is commonly observed after *miR34*-deficient MCCs, whereby ablation of the entire *miR-34/449* family impairs multiciliogenesis (Bao et al., 2012; Song et al., 2014). *miR449* is also known to inhibit the NOTCH pathway to relieve the suppression of multiciliogenesis; however, NOTCH pathway activity in the CP remains unchanged after *miR449* loss. Given the diverse targets of the *miR-34/449* family, it is plausible that *miR449* may enhance MCIDAS/E2F activity independent of NOTCH inhibition. Conversely, transcriptional activation of *miR449* by MCIDAS/E2F complexes may complete the feedback loop to keep the molecular circuit fully engaged in the absence of TAp73.

This interpretation posits that the crosstalk between *miR449* and MCIDAS/E2F serves as a crucial backup for TAp73-driven circuitry in the brain. Indeed, depletion of *miR449* in the absence of *TAp73* results in defective ciliogenesis, indicating that TAp73 functions through miR-34/449 family to generate MCCs in the brain. Of note, complete loss of miR-34/449 family does not recapitulate hydrocephalus phenotype observed in mice lacking both *TAp73* and *miR449* (Fededa et al., 2016; Song et al., 2014). In addition, hydrocephalus and secondary cilia depletion were described for *p73* KO mice lacking all isoforms, but not observed in *TAp73* mutant animals, suggesting a potential role for *ΔNp73* isoforms (Medina-Bolívar et al., 2014; A. Yang et al., 2000). Taken together, the molecular interactome of p73 family in brain ciliogenesis is fascinatingly complex and just beginning to unravel.

Supplementary Material

Figure 5 – Table supplement 1. Summary of sequencing of small RNA species from lateral ventricle/CP of WT (*n*=3) and TAp73$^{-/-}$ (*n*=4) mice. GEO accession number: **GSE108385.**

Figure 2–video supplement 1. Spermatocyte movement in *TAp73*$^{+/-}$ (**A**, **B**) and *TAp73*$^{-/-}$ mice (**C**, **D**).

Figure 3–video supplement 1. Smooth muscle contraction in fallopian tube of WT (**A**) and *TAp73*$^{-/-}$ (**B**) mice.

Figure 4–video supplement 1. Ciliary beating in WT (**A**, 3rd ventricle) and *TAp73*$^{-/-}$ (**B**, lateral ventricle) mice.

Materials and Methods

Animals

TAp73 mutant mice with targeted deletion of exons 2 and 3 of the *Trp73* gene were a generous gift from Dr. Tak Mak (Princess Margaret Cancer Centre, Toronto, Canada) (Tomasini et al., 2008). *miR449* mutants were previously described (Song et al., 2014). Both strains were maintained in C57Bl/6 background (n8) at the animal facility of the European Neuroscience Institute Göttingen, Germany in full compliance with institutional guidelines. The study was approved by the Animal Care Committee of the University Medical Centre Goettingen and the authorities of Lower-Saxony under the number 16/2069.

Human samples

Human epididymis samples were procured with informed consent from two patients (42 and 41 years of age, respectively). All experimental procedures were approved and performed in accordance with the requirements set forth by Ethics Committee of the University Medical Centre Goettingen (application number: 18/2/16).

Histology and immunostaining

Paraformaldehyde-fixed, paraffin-embedded tissues were treated with heat-induced epitope retrieval using Rodent Decloaker (RD913 L, Biocare Medical). For immunohistochemistry, endogenous peroxidase activity was quenched with 3% H_2O_2 for 10 minutes. Tissue sections were blocked with 10% fetal calf serum (FCS) in phosphate buffered saline (PBS) with 0.1% Triton X-100, and subsequently incubated with primary antibody (List of antibodies in **Table 1**). Biotinylated secondary antibodies were applied for 1 hour at room temperature (List of antibodies in **Table 2**), after which avidin enzyme complex and substrate/chromogen were used for color development (Vector laboratories). Stained tissue sections were counterstained with hematoxylin. For immunofluorescence, sections were stained with fluorescently labeled secondary antibodies (**Table 2**) for 1 h at room temperature. Nuclei were counterstained with DAPI.

Table 1. Primary antibody information.

Antibodies	Dilution (Application)	Company	Catalog # [clone]
Mouse monoclonal anti-Ac-α-TUB	1:1000 (IF)	Sigma	T6793 [6-11B-1]
Mouse monoclonal anti- ARL13B	1:500 (IF)	NeuroMab	75-287 [N295B/66]
Rabbit polyclonal anti-ARL13B	1:500 (IHC)	Proteintech	17711-1-AP
Mouse monoclonal anti- AQP1	1:1000 (IHC, IF)	Abcam	ab9566 [1/22]
Rabbit polyclonal anti-AQP1	1:1000 (IF)	EMD Millipore	AB2219
Rabbit polyclonal anti-β-ACTIN	1:10000 (WB)	Abcam	ab8227

Rabbit polyclonal anti-Cytokeratins	1:100 (IHC)	Dako	Z0622
Rabbit polyclonal anti-DNAI1	1:500 (IF); 1:700 (WB)	Sigma	HPA021649
Goat polyclonal anti-DNALI1	1:300 (WB)	Santa Cruz	sc-160296
Rabbit polyclonal anti-FOXJ1	1:500 (WB)	Sigma	HPA005714
Mouse monoclonal anti-HSC70	1:20000 (WB)	Santa Cruz	sc-7298 [B-6]
Rabbit monoclonal anti-KI-67	1:100 (IF)	Abcam	ab16667 [SP6]
Rabbit polyclonal anti-OTX2	1:500 (IHC)	EMD Millipore	AB9566
Rabbit monoclonal anti-P73	1:100 (IF, IHC); 1:300 (WB)	Abcam	ab40658 [EP436Y]
Rabbit polyclonal anti-TTR	1:100 (IHC)	Proteintech	1189-1-AP

Table 2. Secondary antibody information.

Antibodies	**Dilution (Application)**	**Company**	**Catalog #**
Alexa Fluor 488 donkey anti-mouse	1:500 (IF)	Thermo Fisher Scientific	A21202
Alexa Fluor 594 goat anti-rabbit	1:500 (IF)	Thermo Fisher Scientific	A11012
Peroxidase-conjugated donkey anti-mouse	1:10000 (WB)	Jackson Immunoresearch	715-036-150
Peroxidase-conjugated donkey anti-goat	1:10000 (WB)	Jackson Immunoresearch	705-036-147
Peroxidase-conjugated donkey anti-rabbit	1:10000 (WB)	Jackson Immunoresearch	711-036-152
Biotin-SP-conjugated AffiniPure Goat Anti-Rabbit IgG	1:1000 (IHC)	Jackson ImmunoResearch	111-065-144
Biotin-SP-conjugated AffiniPure Donkey Anti-Mouse	1:1000 (IHC)	Jackson ImmunoResearch	715-065-151

568 **Quantification of cilia markers**
569 Cilia were quantified using *ImageJ* software (Schindelin et al., 2012). Briefly, the region of interest
570 was selected and a threshold was set to exclude unspecific background signals. The *Analyze*
571 *Particles* tool was used to measure the area of the ciliary staining. Values were normalized to the
572 length of the epithelia measured.
573
574 **Western blot**
575 Samples were homogenized in RIPA buffer (20 mM TrisHCl pH7.5, 150 mM NaCl, 9.5 mM EDTA,
576 1% Triton X100, 0.1% SDS, 1% sodium desoxycholate) supplemented with urea (2.7 M) and
577 protease inhibitors (Complete Mini EDTA-free, Roche). Equal amounts of protein extracts were
578 separated by SDS-polyacrylamide gels prior to transfer onto a nitrocellulose membrane and
579 incubated with primary antibodies (**Table 1**). The membrane was washed and incubated for 1
580 hour with horse radish peroxidase (HRP)-conjugated secondary antibodies (**Table 2**) followed by
581 chemiluminescence detection. β-actin or heat shock cognate 71 kDa protein (HSC70) was used
582 as protein loading control.
583
584 **RNA extraction, quantitative PCR, *in situ* hybridization, and small RNA sequencing**
585 Tissue samples were snap-frozen in liquid nitrogen and total RNA was isolated by Extrazol
586 (7BioScience)/Chloroform extraction followed by 80% ethanol precipitation at -20°C. For cDNA
587 synthesis, 1µg of total RNA was incubated with the M-MuLV reverse transcriptase and a mix of
588 random nonameric and polyA tail primers at 42°C for 1h in a total volume of 50µl. All reactions
589 were set up in triplicate with self-made SYBR Green qPCR Mix (Tris-HCl [75mM], $(NH4)_2SO_4$
590 [20mM], Tween-20 [0.01% v/v], $MgCl_2$ [3mM], Triton X-100 [0.25% v/v], SYBR Green I (1:40,000),
591 dNTPs [0.2mM] and Taq-polymerase [20U/ml]) using 250nM of each gene-specific primers (**Table**
592 **3**). Standard curve method was used to assess relative transcript content; transcript of interest
593 was normalized to reference transcript of ribosomal phosphoprotein P0 (*Rplp0*, or *36B4*) and
594 normalized to the mean value of control samples. The results for each sample were obtained by
595 averaging transcript levels of technical triplicates. No RT controls and dilution curves as well as
596 melting curves and gel electrophoresis assessment of amplicons were performed for all primer
597 combinations. For *miR-449a* quantification, TaqMan MicroRNA Assay (Thermo Fisher Scientific)
598 was performed according to the manufacturer's instructions with U6 snRNA as internal control.
599
600 *Hes1* (probe no. 417701) and *Hes5* (probe no. 400991-C2) were visualized using RNAscope 2.5
601 HD Duplex Reagent Kit (#322430, Advanced Cell Diagnostics, Hayward, CA) according to
602 manufacturer's instructions.
603
604 The libraries for Small RNA samples were prepared using TruSeq Small RNA Library Prep Kit -
605 Set A (24 rxns) (Set A: indexes 1-12); Cat N°: RS-200-001 using 1 µg of total RNA according to
606 manufactures recommendations. Samples were sequenced on the Illumina HiSeq 4000 using a
607 50 bp single-end approach. Mapping, prediction of novel miRNAs, quality control, and differential
608 expression (DE) analysis were carried out using Oasis2.0 (*Oasis: online analysis of small RNA*
609 *deep sequencing data*) (Capece et al., 2015). In brief, FASTQ files were trimmed with cutadapt
610 1.7.1 (Martin, 2011) removing Truseq adapter sequences (TGGAATTCTCGGGTGCCAAGG)
611 followed by removing sequences smaller than 15 or larger than 32 nucleotides. Trimmed FASTQ

sequences were aligned to mouse sRNAs using STAR version 2.4.1d (Dobin et al., 2013) with a mismatch of 5% of the sequence length and by utilizing the following databases: Mirbase version 21 for microRNA (miRNAs); piRNAbank V.2 for piwiRNA (piRNA); and Ensembl v84 for small nuclear RNA (snRNA), small nucleolar RNA (snoRNA) and ribosomal RNA (rRNA). Counts per small RNA were calculated using featureCounts v1.4.6 (Liao, Smyth, & Shi, 2014). Novel miRNAs were searched for using miRDeep2 version 2.0.0.5 (Friedländer, Mackowiak, Li, Chen, & Rajewsky, 2012). Differential expression of small RNA was determined by DESeq2 (Love, Huber, & Anders, 2014), where sRNAs were considered differentially expressed with an adjusted p-value <0.05 and absolute log2 fold-change >1. The results of the DE analysis can be found in **Figure 5 – Table supplement 1**, and the sRNA-seq data sets can be found in Gene Expression Omnibus (GEO) with accession number **GSE108385**.

Table 3. Sequence information for primers used in RT-qPCR.

Gene	Accession number	Amplicon bp	Exons	Forward primer	Reverse primer
TAp73	NM_011642	163	Ex2-Ex3	5'-AGCAGAATGAGCGGCAGCGTT-3'	5'-TGTTGGACTCCTCGCTGCCTGA-3'
Foxj1	NM_008240	200	Ex2-Ex3	5'-CCATGCAGACCCCACCTGGCA-3'	5'-GGGCAAAGGCAGGGTGGATGT-3'
Dnali1	NM_175223	213	Ex4-Ex5	5'-TTTGGCATGAGGAAGGCACT-3'	5'-CTGGTTGGTCCGTTTCAGGA-3'
Mcidas	NM_001037914	137	Ex7	5'-AACAACGAAAAGGAGCCTGGA-3'	5'-GCCGCTTAGGGTCACGATTG-3'
E2f4	NM_148952	199	Ex7-Ex9	5'-GCACTGGACACTCGGCCT-3'	5'-TGCACTCTCTCGTGGGGTCG-3'
Rfx2	NM_027787	74	Ex5-Ex6	5'-GACGGCACAAGACACTCTCTG-3'	5'-AGAGTCTCAATCGCCATTTCAAG-3'
Rfx3	NM_001360357	107	Ex3	5'-ATGCAGACTTCAGAGACGGGT-3'	5'-ACTGGCACTTGCTGTACCAC-3'
36b4	NM_007475	155	Ex6-Ex7	5'-GCAGATCGGGTACCCAAC-3'	5'-CAGCAGCCGCAAATGCAG-3'

Chromatin immuno-precipitation (ChIP)

Chromatin was harvested from Saos2 cells transiently overexpressing TAp73α, TAp73β and the control vector pcDNA3.1. ChIP and qPCR was performed as previously described using gene specific primers (**Table 4**) (Nemajerova et al., 2016). Enrichment levels were determined as the number of PCR products for each gene relative to total input.

633 **Table 4.** Sequence information for primers used in ChIP-qPCR.

Gene	Forward primer	Reverse primer
FOXJ1 down	5'-CAGCATGCCCAGAAGCTTTG-3'	5'-TCAGGGGCTGCATTCTTCC-3'
FOXJ1 end	5'-AGGGCACACTTAGCCTTTG-3'	5'-AGGAGACAAAGGGAGGAGG-3'
DNAI1	5'-CCCAAGCGGGGTAATCTCT-3'	5'-CTTGAGGTTGTGGGACTTCAC-3'
DNALI1	5'-CACGCCCGGCAAATTTCTG-3'	5'-CAAGGTGGGCAGATCATGTG-3'

634

635 **Luciferase assay**

636 Luciferase assay was performed as previously described (Nemajerova et al., 2016). Briefly,
637 Saos2 cells were transfected with pcDNA3.1 empty vector, or pcDNA3.1 vector carrying *E2F4*, or
638 pcDNA3.1 vector, or both *E2F4* and *MCIDAS* vectors, together with a firefly luciferase reporter
639 construct containing the putative three wild type E2F-binding sequence of *miR449* genomic region
640 (wild type, or "WT"), or the same sequence lacking the strongest predicted E2F-binding motif
641 (mutant, or "Mut") (**Table 5**). In addition, a Renilla TK luciferase vector was co-transfected. At 24
642 hours after transfection, cells were harvested and the luciferase activities were measured using
643 the dual luciferase assay. Firefly luciferase activities were determined relative to those of Renilla
644 TK luciferase vector and normalized to the mean value of samples from control vector.
645

646 **Table 5:** Luciferase constructs for E2F4/MCIDAS reporter assay.

647 RS: Restriction site

Construct name	**DNA sequence of inserts** The strongest E2F binding site is depicted in grey and the removed sequence in **bold underlined**. Two consensus sequences with lower score were retained in the mutant (pink and red).	**Vector**	**5' RS**	**3' RS**
miR449/Cdc20b WT E2F binding site = **WT**	GCCAGAAAGCTGAGCACACTGGGGACTC CGTGATAAAGGGGGAGAGGAAGATATTG AGGGTTGAGGAAGAGGTCTG**GCGGGAAA TGACAGGGAACC**AGATGGGCTGTGCAGC CTTAGCTGCCCATCTGAGCTGCCAAGAGA GCCGAGTTGTGCCATATGGCAGGAG	pGL4.23	NheI	EcoRV
miR449/Cdc20b Mut E2F binding site = **Mut**	GCCAGAAAGCTGAGCACACTGGGGACTC CGTGATAAAGGGGGAGAGGAAGATATTG AGGGTTGAGGAAGAGGTCTGGACAGGGA ACCAGATGGGCTGTGCAGCCTTAGCTGC CCATCTGAGCTGCCAAGAGAGCCGAGTT GTGCCATATGGCAGGAG	pGL4.23	NheI	EcoRV

648
649
650

651 **Video microscopy**
652 Murine fallopian tubes or testis were dissected and transferred to DMEM. Peristaltic contraction
653 of fallopian tube was imaged with an inverse microscope. To image spermatocytes, epididymis
654 was separated from testis and vas deferens. An incision was made at distal end to release to
655 spermatocytes.
656
657 **Imaging of cilia-generated bead-flow and cilia beating in the brain ventricular system**
658 Mouse brains were dissected and transferred to DMEM 21063 (Thermo Fisher Scientific). Lateral
659 ventricle (LV) and ventral third ventricle (v3V) were prepared from a 1mm coronal slice, a 3mm
660 slice, and two 1 mm slices in a coronal adult brain matrix (ASI Instruments) as previously
661 described (Faubel, Westendorf, Bodenschatz, & Eichele, 2016). Tissue explant was placed in
662 DMEM 21063 containing fluorescent latex beads (Fluoresbrite Multifluorescent 1.0 micron
663 Microspheres, Polysciences). Movement of fluorescent beads along the ventricular wall and within
664 ventricular lumen was observed by differential interference contrast (DIC) microscopy using a
665 DMR (Leica) upright microscope with epifluorescence lamp. Bead movement was recorded using
666 a high-speed camera operated by MultiRecorder Software (Cascade II-512, Photometrics) and
667 analyzed using ImageJ software (Schindelin et al., 2012).
668
669 **Statistical Analysis**
670 One-tailed, unpaired Student's test assuming normal distribution was used to calculate statistical
671 significance for pairwise comparisons. Luciferase assay statistics were assessed using one-way
672 ANOVA assuming normal distribution followed by Bunnett's multiple comparison tests. The
673 following indications of significance were used: *P<0.05, ** P <0.01, *** P <0.005. N values
674 represent biological replicates. Error bars indicate standard error of the mean (SEM).
675
676
677
678 **Acknowledgments**
679 We thank Tak Mak for providing *TAp73* KO mice, Gerd Hasenfuss for support, Matthias
680 Dobbelstein for hosting and Karola Metze, Verena Siol and Sabine Bolte for assistance. M.L. is
681 supported by Deutsche Forschungsgemeinschaft (DFG Li 2405); H.Z. by New York Institute of
682 Technology, Sanford Research, Matthew Larson Foundation, Institutional Development Award
683 from the National Institute of General Medical Sciences under grant numbers 5P20GM103548,
684 1P20GM103620-01A1, and National Cancer Institute (R01CA220551); F.B. by Wilhelm-Sander-
685 Stiftung (2016.041.1); A.K.G by the Max Planck Society. We thank Heymut Omran's group for
686 introduction to cilia microscopy and Travis Stracker for disclosure of non-published data.

687

688 **Author Contributions**
689 T.E. and Me.W. characterized cilia defects and gene expression and generated figures. Me.W.
690 and Ma.W. validated TAp73 targets by WB and ChIP. E.E. and F.B. contributed IF analysis of
691 human epididymis. C.W. maintained mice, performed RNA isolation and qPCRs. K.B.G., J.Z., L.L.
692 and H.Z. contributed brain analyzes. O.S. analyzed small RNA sequencing data. S.A. contributed
693 to interpretation and supported the group. M.L. developed the project, interpreted the data,

694 designed and coordinated the experiments to complete this study. Me.W., T.E., H.Z. and M.L.
695 were major contributors to manuscript preparation.

696

697 **Competing Financial Interest Statement**
698 The authors declare no competing financial interests.

699
700

References

Amirav, I., Wallmeier, J., Loges, N. T., Menchen, T., Pennekamp, P., Mussaffi, H., … Israeli PCD Consortium Investigators. (2016). Systematic Analysis of CCNO Variants in a Defined Population: Implications for Clinical Phenotype and Differential Diagnosis. *Human Mutation*, *37*(4), 396–405. https://doi.org/10.1002/humu.22957

Arbi, M., Pefani, D.-E., Kyrousi, C., Lalioti, M.-E., Kalogeropoulou, A., Papanastasiou, A. D., … Lygerou, Z. (2016). GemC1 controls multiciliogenesis in the airway epithelium. *EMBO Reports*, *17*(3), 400–413. https://doi.org/10.15252/embr.201540882

Bao, J., Li, D., Wang, L., Wu, J., Hu, Y., Wang, Z., … Xu, C. (2012). MicroRNA-449 and MicroRNA-34b/c Function Redundantly in Murine Testes by Targeting E2F Transcription Factor-Retinoblastoma Protein (E2F-pRb) Pathway. *Journal of Biological Chemistry*, *287*(26), 21686–21698. https://doi.org/10.1074/jbc.M111.328054

Bill, B. R., Balciunas, D., McCarra, J. A., Young, E. D., Xiong, T., Spahn, A. M., … Schimmenti, L. A. (2008). Development and Notch Signaling Requirements of the Zebrafish Choroid Plexus. *PLoS ONE*, *3*(9), e3114. https://doi.org/10.1371/journal.pone.0003114

Blatt, E. N., Yan, X. H., Wuerffel, M. K., Hamilos, D. L., & Brody, S. L. (1999). Forkhead transcription factor HFH-4 expression is temporally related to ciliogenesis. *American Journal of Respiratory Cell and Molecular Biology*, *21*(2), 168–176. https://doi.org/10.1165/ajrcmb.21.2.3691

Boon, M., Wallmeier, J., Ma, L., Loges, N. T., Jaspers, M., Olbrich, H., … Omran, H. (2014). MCIDAS mutations result in a mucociliary clearance disorder with reduced generation of multiple motile cilia. *Nature Communications*, *5*, 4418. https://doi.org/10.1038/ncomms5418

Brody, S. L., Yan, X. H., Wuerffel, M. K., Song, S. K., & Shapiro, S. D. (2000). Ciliogenesis and left-right axis defects in forkhead factor HFH-4-null mice. *American Journal of Respiratory Cell and Molecular Biology*, *23*(1), 45–51. https://doi.org/10.1165/ajrcmb.23.1.4070

Capece, V., Garcia Vizcaino, J. C., Vidal, R., Rahman, R.-U., Pena Centeno, T., Shomroni, O., … Bonn, S. (2015). Oasis: online analysis of small RNA deep sequencing data. *Bioinformatics*, *31*(13), 2205–2207. https://doi.org/10.1093/bioinformatics/btv113

Caspary, T., Larkins, C. E., & Anderson, K. V. (2007). The Graded Response to Sonic Hedgehog Depends on Cilia Architecture. *Developmental Cell*, *12*(5), 767–778. https://doi.org/10.1016/j.devcel.2007.03.004

Chen, J., Knowles, H. J., Hebert, J. L., & Hackett, B. P. (1998). Mutation of the mouse hepatocyte nuclear factor/forkhead homologue 4 gene results in an absence of cilia and random left-right asymmetry. *The Journal of Clinical Investigation*, *102*(6), 1077–1082. https://doi.org/10.1172/JCI4786

Choksi, S. P., Lauter, G., Swoboda, P., & Roy, S. (2014). Switching on cilia: transcriptional networks regulating ciliogenesis. *Development (Cambridge, England)*, *141*(7), 1427–1441. https://doi.org/10.1242/dev.074666

Crow, J., Amso, N. N., Lewin, J., & Shaw, R. W. (1994). Morphology and ultrastructure of fallopian tube epithelium at different stages of the menstrual cycle and menopause. *Human Reproduction (Oxford, England)*, *9*(12), 2224–2233.

739 Dacheux, J.-L., & Dacheux, F. (2013). New insights into epididymal function in relation to sperm
740 maturation. *Reproduction*, *147*(2), R27–R42. https://doi.org/10.1530/REP-13-0420

741 Danielian, P. S., Bender Kim, C. F., Caron, A. M., Vasile, E., Bronson, R. T., & Lees, J. A. (2007). E2f4 is
742 required for normal development of the airway epithelium. *Developmental Biology*, *305*(2), 564–576.
743 https://doi.org/10.1016/j.ydbio.2007.02.037

744 Danielian, P. S., Hess, R. A., & Lees, J. A. (2016). E2f4 and E2f5 are essential for the development of the
745 male reproductive system. *Cell Cycle (Georgetown, Tex.)*, *15*(2), 250–260.
746 https://doi.org/10.1080/15384101.2015.1121350

747 Del Bigio, M. R. (2010). Ependymal cells: biology and pathology. *Acta Neuropathologica*, *119*(1), 55–73.
748 https://doi.org/10.1007/s00401-009-0624-y

749 Diez-Roux, G., Banfi, S., Sultan, M., Geffers, L., Anand, S., Rozado, D., … Ballabio, A. (2011). A High-
750 Resolution Anatomical Atlas of the Transcriptome in the Mouse Embryo. *PLoS Biology*, *9*(1), e1000582.
751 https://doi.org/10.1371/journal.pbio.1000582

752 Dobin, A., Davis, C. A., Schlesinger, F., Drenkow, J., Zaleski, C., Jha, S., … Gingeras, T. R. (2013). STAR:
753 ultrafast universal RNA-seq aligner. *Bioinformatics (Oxford, England)*, *29*(1), 15–21.
754 https://doi.org/10.1093/bioinformatics/bts635

755 Faubel, R., Westendorf, C., Bodenschatz, E., & Eichele, G. (2016). Cilia-based flow network in the brain
756 ventricles. *Science*, *353*(6295), 176–178. https://doi.org/10.1126/science.aae0450

757 Fededa, J. P., Esk, C., Mierzwa, B., Stanyte, R., Yuan, S., Zheng, H., … Gerlich, D. W. (2016). MicroRNA-
758 34/449 controls mitotic spindle orientation during mammalian cortex development. *The EMBO Journal*,
759 *35*(22), 2386–2398. https://doi.org/10.15252/embj.201694056

760 Feng, Z., Zhang, C., Kang, H.-J., Sun, Y., Wang, H., Naqvi, A., … Hu, W. (2011). Regulation of female
761 reproduction by p53 and its family members. *FASEB Journal: Official Publication of the Federation of*
762 *American Societies for Experimental Biology*, *25*(7), 2245–2255. https://doi.org/10.1096/fj.10-180166

763 Friedländer, M. R., Mackowiak, S. D., Li, N., Chen, W., & Rajewsky, N. (2012). miRDeep2 accurately
764 identifies known and hundreds of novel microRNA genes in seven animal clades. *Nucleic Acids Research*,
765 *40*(1), 37–52. https://doi.org/10.1093/nar/gkr688

766 Guglielmino, M. R., Santonocito, M., Vento, M., Ragusa, M., Barbagallo, D., Borzì, P., … Di Pietro, C.
767 (2011). TAp73 is downregulated in oocytes from women of advanced reproductive age. *Cell Cycle*
768 *(Georgetown, Tex.)*, *10*(19), 3253–3256. https://doi.org/10.4161/cc.10.19.17585

769 Hess, R. A. (2002). The Efferent Ductules: Structure and Functions. In B. Robaire & B. T. Hinton (Eds.),
770 *The Epididymis: From Molecules to Clinical Practice* (pp. 49–80). Boston, MA: Springer US. Retrieved
771 from http://link.springer.com/10.1007/978-1-4615-0679-9_4

772 Holembowski, L., Kramer, D., Riedel, D., Sordella, R., Nemajerova, A., Dobbelstein, M., & Moll, U. M.
773 (2014). TAp73 is essential for germ cell adhesion and maturation in testis. *The Journal of Cell Biology*,
774 *204*(7), 1173–1190. https://doi.org/10.1083/jcb.201306066

775 Hu, W., Zheng, T., & Wang, J. (2011). Regulation of Fertility by the p53 Family Members. *Genes &*
776 *Cancer*, *2*(4), 420–430. https://doi.org/10.1177/1947601911408892

Ilio, K. Y., & Hess, R. A. (1994). Structure and function of the ductuli efferentes: a review. *Microscopy Research and Technique*, *29*(6), 432–467. https://doi.org/10.1002/jemt.1070290604

Inoue, S., Tomasini, R., Rufini, A., Elia, A. J., Agostini, M., Amelio, I., … Mak, T. W. (2014). TAp73 is required for spermatogenesis and the maintenance of male fertility. *Proceedings of the National Academy of Sciences*, *111*(5), 1843–1848. https://doi.org/10.1073/pnas.1323416111

Koeppel, M., van Heeringen, S. J., Kramer, D., Smeenk, L., Janssen-Megens, E., Hartmann, M., … Lohrum, M. (2011). Crosstalk between c-Jun and TAp73alpha/beta contributes to the apoptosis-survival balance. *Nucleic Acids Research*, *39*(14), 6069–6085. https://doi.org/10.1093/nar/gkr028

Kyrousi, C., Lalioti, M.-E., Skavatsou, E., Lygerou, Z., & Taraviras, S. (2016). Mcidas and GemC1/Lynkeas specify embryonic radial glial cells. *Neurogenesis*, *3*(1), e1172747. https://doi.org/10.1080/23262133.2016.1172747

Lambot, M.-A. H., Mendive, F., Laurent, P., Van Schoore, G., Noël, J.-C., Vanderhaeghen, P., & Vassart, G. (2009). Three-dimensional reconstruction of efferent ducts in wild-type and Lgr4 knock-out mice. *Anatomical Record (Hoboken, N.J.: 2007)*, *292*(4), 595–603. https://doi.org/10.1002/ar.20883

Li, L., Grausam, K. B., Wang, J., Lun, M. P., Ohli, J., Lidov, H. G. W., … Zhao, H. (2016). Sonic Hedgehog promotes proliferation of Notch-dependent monociliated choroid plexus tumour cells. *Nature Cell Biology*, *18*(4), 418–430. https://doi.org/10.1038/ncb3327

Liao, Y., Smyth, G. K., & Shi, W. (2014). featureCounts: an efficient general purpose program for assigning sequence reads to genomic features. *Bioinformatics (Oxford, England)*, *30*(7), 923–930. https://doi.org/10.1093/bioinformatics/btt656

Lindeman, G. J., Dagnino, L., Gaubatz, S., Xu, Y., Bronson, R. T., Warren, H. B., & Livingston, D. M. (1998). A specific, nonproliferative role for E2F-5 in choroid plexus function revealed by gene targeting. *Genes & Development*, *12*(8), 1092–1098.

Lizé, M., Herr, C., Klimke, A., Bals, R., & Dobbelstein, M. (2010). MicroRNA-449a levels increase by several orders of magnitude during mucociliary differentiation of airway epithelia. *Cell Cycle (Georgetown, Tex.)*, *9*(22), 4579–4583. https://doi.org/10.4161/cc.9.22.13870

Lizé, M., Pilarski, S., & Dobbelstein, M. (2010). E2F1-inducible microRNA 449a/b suppresses cell proliferation and promotes apoptosis. *Cell Death and Differentiation*, *17*(3), 452–458. https://doi.org/10.1038/cdd.2009.188

Love, M. I., Huber, W., & Anders, S. (2014). Moderated estimation of fold change and dispersion for RNA-seq data with DESeq2. *Genome Biology*, *15*(12), 550. https://doi.org/10.1186/s13059-014-0550-8

Lun, M. P., Johnson, M. B., Broadbelt, K. G., Watanabe, M., Kang, Y. -j., Chau, K. F., … Lehtinen, M. K. (2015). Spatially Heterogeneous Choroid Plexus Transcriptomes Encode Positional Identity and Contribute to Regional CSF Production. *Journal of Neuroscience*, *35*(12), 4903–4916. https://doi.org/10.1523/JNEUROSCI.3081-14.2015

Lun, M. P., Monuki, E. S., & Lehtinen, M. K. (2015). Development and functions of the choroid plexus-cerebrospinal fluid system. *Nature Reviews Neuroscience*, *16*(8), 445–457. https://doi.org/10.1038/nrn3921

Lyons, R. A., Saridogan, E., & Djahanbakhch, O. (2006). The reproductive significance of human Fallopian tube cilia. *Human Reproduction Update*, *12*(4), 363–372. https://doi.org/10.1093/humupd/dml012

Ma, L., Quigley, I., Omran, H., & Kintner, C. (2014). Multicilin drives centriole biogenesis via E2f proteins. *Genes & Development*, *28*(13), 1461–1471. https://doi.org/10.1101/gad.243832.114

Marcet, B., Chevalier, B., Coraux, C., Kodjabachian, L., & Barbry, P. (2011). MicroRNA-based silencing of Delta/Notch signaling promotes multiple cilia formation. *Cell Cycle*, *10*(17), 2858–2864. https://doi.org/10.4161/cc.10.17.17011

Marcet, B., Chevalier, B., Luxardi, G., Coraux, C., Zaragosi, L.-E., Cibois, M., … Barbry, P. (2011). Control of vertebrate multiciliogenesis by miR-449 through direct repression of the Delta/Notch pathway. *Nature Cell Biology*, *13*(6), 693–699. https://doi.org/10.1038/ncb2241

Marshall, C. B., Mays, D. J., Beeler, J. S., Rosenbluth, J. M., Boyd, K. L., Santos Guasch, G. L., … Pietenpol, J. A. (2016). p73 Is Required for Multiciliogenesis and Regulates the Foxj1-Associated Gene Network. *Cell Reports*, *14*(10), 2289–2300. https://doi.org/10.1016/j.celrep.2016.02.035

Martin, M. (2011). Cutadapt removes adapter sequences from high-throughput sequencing reads. *EMBnet.journal*, *17*(1), 10. https://doi.org/10.14806/ej.17.1.200

Medina-Bolívar, C., González-Arnay, E., Talos, F., González-Gómez, M., Moll, U. M., & Meyer, G. (2014). Cortical hypoplasia and ventriculomegaly of p73-deficient mice: Developmental and adult analysis: p73 in developing and adult cortex. *Journal of Comparative Neurology*, *522*(11), 2663–2679. https://doi.org/10.1002/cne.23556

Mori, M., Hazan, R., Danielian, P. S., Mahoney, J. E., Li, H., Lu, J., … Cardoso, W. V. (2017). Cytoplasmic E2f4 forms organizing centres for initiation of centriole amplification during multiciliogenesis. *Nature Communications*, *8*, 15857. https://doi.org/10.1038/ncomms15857

Nemajerova, A., Kramer, D., Siller, S. S., Herr, C., Shomroni, O., Pena, T., … Lizé, M. (2016). TAp73 is a central transcriptional regulator of airway multiciliogenesis. *Genes & Development*, *30*(11), 1300–1312. https://doi.org/10.1101/gad.279836.116

Pefani, D.-E., Dimaki, M., Spella, M., Karantzelis, N., Mitsiki, E., Kyrousi, C., … Lygerou, Z. (2011). Idas, a Novel Phylogenetically Conserved Geminin-related Protein, Binds to Geminin and Is Required for Cell Cycle Progression. *Journal of Biological Chemistry*, *286*(26), 23234–23246. https://doi.org/10.1074/jbc.M110.207688

Raidt, J., Werner, C., Menchen, T., Dougherty, G. W., Olbrich, H., Loges, N. T., … Omran, H. (2015). Ciliary function and motor protein composition of human fallopian tubes. *Human Reproduction (Oxford, England)*, *30*(12), 2871–2880. https://doi.org/10.1093/humrep/dev227

Redshaw, N., Wheeler, G., Hajihosseini, M. K., & Dalmay, T. (2009). microRNA-449 is a putative regulator of choroid plexus development and function. *Brain Research*, *1250*, 20–26. https://doi.org/10.1016/j.brainres.2008.11.020

Schindelin, J., Arganda-Carreras, I., Frise, E., Kaynig, V., Longair, M., Pietzsch, T., … Cardona, A. (2012). Fiji: an open-source platform for biological-image analysis. *Nature Methods*, *9*(7), 676–682. https://doi.org/10.1038/nmeth.2019

853 Silva-Vargas, V., Maldonado-Soto, A., Mizrak, D., Codega, P., & Doetsch, F. (2016). Age-Dependent Niche
854 Signals from the Choroid Plexus Regulate Adult Neural Stem Cells. *Cell Stem Cell*, *19*(5), 643–652.
855 https://doi.org/10.1016/j.stem.2016.06.013

856 Song, R., Walentek, P., Sponer, N., Klimke, A., Lee, J. S., Dixon, G., … He, L. (2014). miR-34/449 miRNAs
857 are required for motile ciliogenesis by repressing cp110. *Nature*, *510*(7503), 115–120.
858 https://doi.org/10.1038/nature13413

859 Spassky, N., Merkle, F. T., Flames, N., Tramontin, A. D., García-Verdugo, J. M., & Alvarez-Buylla, A.
860 (2005). Adult ependymal cells are postmitotic and are derived from radial glial cells during
861 embryogenesis. *The Journal of Neuroscience: The Official Journal of the Society for Neuroscience*, *25*(1),
862 10–18. https://doi.org/10.1523/JNEUROSCI.1108-04.2005

863 Spassky, N., & Meunier, A. (2017). The development and functions of multiciliated epithelia. *Nature*
864 *Reviews Molecular Cell Biology*, *18*(7), 423–436. https://doi.org/10.1038/nrm.2017.21

865 Stubbs, J. L., Vladar, E. K., Axelrod, J. D., & Kintner, C. (2012). Multicilin promotes centriole assembly and
866 ciliogenesis during multiciliate cell differentiation. *Nature Cell Biology*, *14*(2), 140–147.
867 https://doi.org/10.1038/ncb2406

868 Terré, B., Piergiovanni, G., Segura-Bayona, S., Gil-Gómez, G., Youssef, S. A., Attolini, C. S.-O., … Stracker,
869 T. H. (2016). GEMC1 is a critical regulator of multiciliated cell differentiation. *The EMBO Journal*, *35*(9),
870 942–960. https://doi.org/10.15252/embj.201592821

871 Tomasini, R., Tsuchihara, K., Wilhelm, M., Fujitani, M., Rufini, A., Cheung, C. C., … Mak, T. W. (2008).
872 TAp73 knockout shows genomic instability with infertility and tumor suppressor functions. *Genes &*
873 *Development*, *22*(19), 2677–2691. https://doi.org/10.1101/gad.1695308

874 Vanaken, G. J., Bassinet, L., Boon, M., Mani, R., Honoré, I., Papon, J.-F., … Christin-Maitre, S. (2017).
875 Infertility in an adult cohort with primary ciliary dyskinesia: phenotype–gene association. *European*
876 *Respiratory Journal*, *50*(5), 1700314. https://doi.org/10.1183/13993003.00314-2017

877 Yang, A., Walker, N., Bronson, R., Kaghad, M., Oosterwegel, M., Bonnin, J., … Caput, D. (2000). p73-
878 deficient mice have neurological, pheromonal and inflammatory defects but lack spontaneous tumours.
879 *Nature*, *404*(6773), 99–103. https://doi.org/10.1038/35003607

880 Yang, X., Feng, M., Jiang, X., Wu, Z., Li, Z., Aau, M., & Yu, Q. (2009). miR-449a and miR-449b are direct
881 transcriptional targets of E2F1 and negatively regulate pRb-E2F1 activity through a feedback loop by
882 targeting CDK6 and CDC25A. *Genes & Development*, *23*(20), 2388–2393.
883 https://doi.org/10.1101/gad.1819009

884 Yu, X., Ng, C. P., Habacher, H., & Roy, S. (2008). Foxj1 transcription factors are master regulators of the
885 motile ciliogenic program. *Nature Genetics*, *40*(12), 1445–1453. https://doi.org/10.1038/ng.263

886 Zhou, F., Narasimhan, V., Shboul, M., Chong, Y. L., Reversade, B., & Roy, S. (2015). Gmnc Is a Master
887 Regulator of the Multiciliated Cell Differentiation Program. *Current Biology*, *25*(24), 3267–3273.
888 https://doi.org/10.1016/j.cub.2015.10.062

889